Plant-Necrotroph Co-transcriptome Networks Illuminate a Metabolic Battlefield

Wei Zhang[1,2], Jason A. Corwin[3], Daniel Copeland[2], Julie Feusier[2], Robert Eshbaugh[2], David E. Cook[1], Susana Atwell[2], and Daniel J. Kliebenstein[2,4*]

[1]Department of Plant Pathology, Kansas State University, 1712 Clafflin Road, Throckmorton Hall, Manhattan, KS, 66506, USA

[2]Department of Plant Sciences, University of California, Davis, One Shields Avenue, Davis, CA, 95616, USA

[3]Department of Ecology and Evolution Biology, University of Colorado, 1900 Pleasant Street, 334 UCB, Boulder, CO, 80309-0334, USA

[4]DynaMo Center of Excellence, University of Copenhagen, Thorvaldsensvej 40, DK-1871, Frederiksberg C, Denmark

***Correspondence:** Daniel J. Kliebenstein, Department of Plant Sciences, University of California, Davis, One Shields Ave, Davis, CA, 95616, USA.

kliebenstein@ucdavis.edu

Phone: 530-754-7775

Running title: Co-transcriptome Networks between Arabidopsis and *Botrytis cinerea*

Keywords: Host-pathogen Interaction, Pathosystem, Arabidopsis, *B. cinerea*, RNA-Seq, Gene Co-expression Network, Co-transcriptome

Abstract

A central goal of studying host-pathogen interaction research is to understand how the host and pathogen manipulate each other to promote their own fitness in a pathosystem. Co-transcriptomic approaches can simultaneously analyze dual transcriptomes during infection and provide a systematic map of the cross-kingdom communication between two species. Here we used the Arabidopsis-*B. cinerea* pathosystem to test how plant host and fungal pathogen interaction at the transcriptomic level during infection. We assessed the impact of natural genetic diversity in the pathogen and plant host by utilization of a collection of 96 isolates of *B. cinerea* infection on Arabidopsis wild-type and two mutants with jasmonate or salicylic acid compromised immunities. We identified ten *B. cinerea* gene co-expression networks (GCNs) that encode known or novel virulence mechanisms. We constructed a dual interaction network by combining four host- and ten pathogen-GCNs into a single network, which revealed potential connections between the fungal and plant GCNs involving both novel and conserved mechanisms. These co-transcriptome data shed lights on the potential mechanisms underlying host-pathogen interaction and illustrate the continued need for advancements of *in planta* analysis of dual-species dynamics.

INTRODUCTION

How a host and pathogen manipulate each other within a pathosystem to facilitate their own fitness remains a long-standing question. The difference between the pathogen's ability to infect and the host's ability to resist generates the resulting disease symptomology. This interaction forces host-pathogen dynamics to shape the genomes of the two species via adaptive respionses to each other (Dangl and Jones, 2001; Bergelson et al., 2001; Benton, 2009; Kanzaki et al., 2012; Karasov et al., 2014). Plants have evolved a sophisticated set of constitutive and inducible immune responses to cope with constant selective pressures from antagonistic microbes (Jones and Dangl, 2006). Reciprocally, plant pathogens have also evolved a variety of different invasion and virulence strategies to disarm or circumvent plant defense strategies (Glazebrook, 2005; Toruno et al., 2016). This has resulted in complex relations between plant hosts and fungal pathogens for survival and fitness.

The plant innate immune system includes several functional layers with overlapping functions to detect and defend against phytopathogens. This multi-layer immune system can be categorized as a signal monitor system to detect invasion, local and systemic signal transduction components to elicit and coordinate responses, and defensive response proteins and metabolites focused on combatting the invading pathogen (Tsuda and Katagiri, 2010; Corwin and Kliebenstein, 2017). These functional layers, as well as the components within them, are highly interconnected and tightly regulated by the host plant to respond appropriately to various phytopathogens (Couto and Zipfel, 2016; Tang et al., 2017). For instance, Arabidopsis utilizes a complex signaling network to regulate the production of indole-derived secondary metabolites, such as camalexin and indole glucosinolates, that contribute to resistance against pathogens (Kliebenstein et al., 2005; Clay et al., 2009; Bednarek et al., 2009; Frerigmann et al., 2016; Xu et al., 2016; Mine et al., 2018). This layered immune system provides pathogens with numerous targets in the plant immune system that the pathogen can utilize, evade or attack. Most biotrophic pathogens, evolved from commensal microbes, attempt to dismantle the plant immune system by injecting effector proteins into host cells or the inter-cellular space (Dangl and Jones, 2001; Buttner and He, 2009; Stergiopoulos and de Wit, 2009). For example, the biotrophic bacterial pathogen *Pseudomonas syringae* can utilize the jasmonic acid (JA) signaling pathway through the production of a JA-mimic, coronatine, to enhance its fitness (Mittal and Davis, 1995; Brooks et al., 2005; Cui et al., 2018). Alternatively, necrotrophic pathogens, which often evolved from

environmental saprophytic microbes, can utilize toxic secondary metabolites, small secreted proteins, and small RNAs to aggressively attack host defenses while also defending against host-derived toxins (Choquer et al., 2007; Arbelet et al., 2010; Mengiste, 2012; Weiberg et al., 2013; Kubicek et al., 2014; Macheleidt et al., 2016). In addition, pathogens can directly resist downstream defenses as is done by *B. cinerea*, where it has an ATP-binding cassette (ABC) transporter BcatrB that provides resistance by exporting camalexin from the pathogen cell (Stefanato et al., 2009). This high level of interactivity between the immune system and pathogen virulence mechanisms generates the final level of disease severity. However, a functional description of this combative cross-kingdom communication between a plant host and necrotrophic pathogen remains elusive.

Co-transcriptomic approaches whereby the host and pathogen transcriptomes are simultaneously analyzed provide the ability to systematically map the cross-kingdom communication between plant hosts and their pathogens, both for individual genes and gene co-expression network (GCN) levels (Stuart et al., 2003; Musungu et al., 2016; Zhang et al., 2017; Lanver et al., 2018; McClure et al., 2018). Recent advances have enabled the measurement of pathogen *in planta* transcriptome. For example, co-transcriptome work within the biotrophic Arabidopsis-*Pseudomonas syringae* pathosystem has enabled the investigation of early effects on Arabidopsis host immunity and the consequent effects on bacterial growth (Nobori et al., 2018). The co-transcriptome methodology enabled the identification of a bacterial iron acquisition pathway that is suppressed by multiple plant immune pathways (Nobori et al., 2018). This shows the potential for new hypothesis to be generated by a co-transcriptome approach, but additional cases across diverse pathosystems are needed (Swierzy et al., 2017; Westermann et al., 2017; Lee et al., 2018).

The Arabidopsis-*B. cinerea* pathosystem is well suited for exploring plant-pathogen interaction to understand host defenses and necrotrophic virulence in ecological and agricultural settings. *B. cinerea* is a necrotrophic generalist pathogen that attacks a broad range of diverse plant hosts, including dicots, gymnosperms, and even bryophytes (Williamson et al., 2007). This necrotrophic pathogen is endemic throughout the world and can cause severe pre- and post-harvest losses in many crops. A high level of standing natural genetic variation within *B. cinerea* population is hypothesized to facilitate the extreme host range of *B. cinerea*. This genetic variation affects nearly all known *B. cinerea* virulence strategies, including penetration and

112 establishment, evading detection, and combatting/coping with plant immune responses (Atwell
113 et al., 2015; Walker et al., 2015; Corwin, Subedy et al., 2016). For example, a key virulence
114 mechanism is the secretion of phytotoxic secondary metabolites, including the sesquiterpene
115 botrydial (BOT) and the polyketide botcinic acid (BOA) that trigger plant chlorosis and host cell
116 collapse (Deighton et al., 2001; Colmenares et al., 2002; Wang et al., 2009; Rossi et al., 2011;
117 Ascari et al., 2013; Porquier et al., 2016). These metabolites are linked to virulence, but some
118 pathogenic field isolates fail to produce either compounds pointing to additional pathogenic
119 strategies. The combination of a high level of genetic diversity and extensive recombination
120 means that a population of *B. cinerea* is a mixed collection of virulence strategies that can be
121 used to interrogate by the co-transcriptome.

122 In the present study, we used the Arabidopsis-*B. cinerea* pathosystem to test how the
123 transcriptomes of the two species interact during infection and assess how natural genetic
124 variation in the pathogen impacts disease development. Isolates were inoculated on Arabidopsis
125 Col-0 wild-type (WT) in conjunction with immune-deficient hormone mutants *coi1-1* (jasmonate
126 defense signaling) and *npr1-1* (salicylic acid defense signaling). For the pathogen, we utilized a
127 collection of 96 isolates of *B. cinerea* that harbor a wide scope of natural genetic variation within
128 the species (Atwell et al., 2015; Corwin, Subedy et al., 2016; Zhang et al., 2016; Corwin,
129 Copeland et al., 2016; Zhang et al., 2017; Soltis et al., 2018; Fordyce et al., 2018). From
130 individual infected leaves, we simultaneously measured both the Arabidopsis and *B. cinerea*
131 transcripts at 16 hours post-infection (HPI). We have previously analyzed the Arabidopsis
132 transcripts to identify four host-derived GCNs that are sensitive to natural genetic variation in *B.*
133 *cinerea* (Zhang et al., 2017). In present analysis, we identified ten fungal pathogen-derived
134 GCNs that encode either known or novel virulence mechanisms within the species. Some of
135 these *B. cinerea* GCNs responsible for BOT production, exocytosis regulation and copper
136 transport are highly linked with the host's defense phytohormone pathways. By combining the
137 plant host- and pathogen-GCNs into a single network, we constructed a dual-transcriptomic
138 network that identifies potential interactions between the components of plant host innate
139 immune system and fungal pathogen virulence. These connections highlight potential targets for
140 fungal pathogen phytotoxins and prevailing counter-responses from plant host. Collectively,
141 these data shed lights on the potential mechanisms underlying how the host and pathogen combat
142 each other during infection and illustrate the continued need for advancements of *in planta*
143 analysis of dual-species interaction.

RESULTS

Genetic Variation in Pathogen and Hosts Influence *B. cinerea* Transcriptome

To investigate how genetic variation within a pathogen differentially interacts with plant host immunity at the transcriptomic level, we profiled the *in planta* transcriptomes of 96 *B. cinerea* isolates infection across three host genotypes, the Arabidopsis accession Col-0 WT and two immune-signaling mutants *coi1-1* and *npr1-1* that are respectively compromised in JA or salicylic acid (SA) driven immunity. This previously described collection of 96 isolates represents a broad geographical distribution and contains considerable natural genetic variation that affects a diversity of virulence strategies within *B. cinerea* (Denby et al., 2004; Rowe and Kliebenstein, 2007; Atwell et al., 2015; Corwin, Subedy et al., 2016; Zhang et al., 2016). Four independent biological replicates across two separate experiments per isolate/genotype pair were harvested at 16 HPI for transcriptome analysis. A total of 1,152 independent RNA samples were generated for library preparation and sequenced on Illumina HiSeq platform (NCBI accession number SRP149815). These libraries were previously used to study Arabidopsis transcriptional responses to natural genetic variation in *B. cinerea* (Zhang et al., 2017). Mapping the dual-transcriptome reads against the *B. cinerea* reference genome (B05.10), we identified 9,284 predicted gene models with a minimum of either 30 gene counts in one isolate or 300 gene counts across 96 isolates. The total of identified genes corresponds to ~79% of the 11,701 predicted encoding genes in B05.10 reference genome (Supplemental Data Set 1 to 3) (Van Kan et al., 2017). The two different thresholds allowed the identification of pathogen transcripts that express only in a specific isolate.

Measuring the abundance of individual pathogen transcripts in relation to the host transcripts can be used as a molecular method to estimate fungal biomass (Blanco-Ulate et al., 2014). Given this, we hypothesized that the fraction of total reads that map to *B. cinerea* might be a biologically relevant indicator of pathogen virulence (Supplemental Data Set 4). Comparing *B. cinerea* transcript abundance at 16 HPI to lesion development at 72 HPI revealed a significant partial correlation in the WT Col-0 (R^2 = 0.1101, *P*-value = 0.0016, Figure 1). In contrast to WT, the early transcriptomic activities of most *B. cinerea* isolates were more vigorous in the two Arabidopsis mutants, resulting in a significant curvilinear relationship between total fraction of *B. cinerea* reads and final lesion area (*P*-value = 3.914e-07, *P*-value = 0.0001, respectively,

Figure 1). Interestingly, the total reads fraction was better correlated with final lesion area in *coi1-1* (R^2= 0.2562) than either WT (R^2 = 0.1101) or *npr1-1* (R^2 = 0.161). This suggests that early transcriptomic activity from the pathogen can be a partial indicator of pathogen virulence, but also depends on the respective resistance from the plant host.

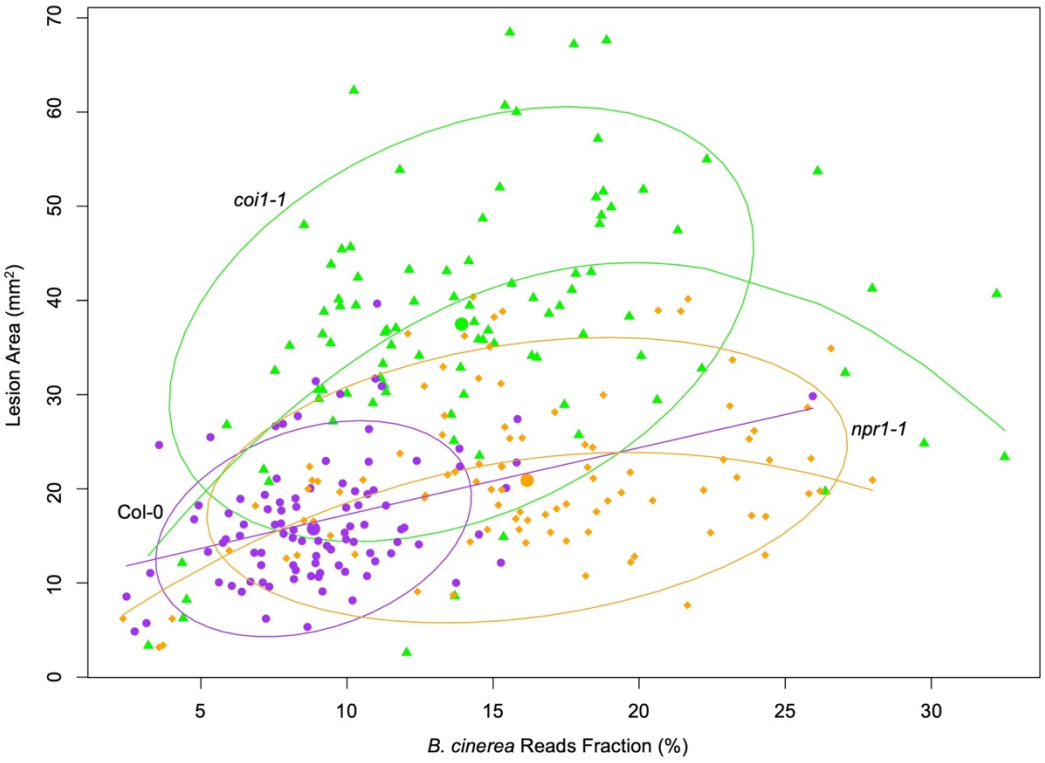

Figure 1. Correlation between earlier estimated *B. cinerea* biomass and later lesion area. Model-corrected lesion area means were estimated using the linear model on the six replicates data from three Arabidopsis genotypes at 72-hours post-infection with 96 *B. cinerea* isolates. Estimated biomass of *B. cinerea* was calculated using the linear model-corrected fraction of *B. cinerea* mapped reads against total mapped reads to Arabidopsis and *B. cinerea* reference genomes. RNA-Seq analysis was conducted at 16-hours post-infection for each pathosystem. Three Arabidopsis genotypes are wild-type Col-0 (purple dot), jasmonate insensitive mutant *coi1-1* (green triangle), and salicylic acid insensitive mutant *npr1-1* (orange diamond). The 90% confidence ellipse intervals are plotted for each Arabidopsis genotype for references. Quadratic regression lines are: Col-0: $y = -0.00059x^2 + 0.729x + 10.037$, $P = 0.0016$, adjusted $R^2 = 0.1101$; *coi1-1*: $y = -0.117x^2 + 4.44x - 0.1585$, $P = 3.914e-07$, adjusted $R^2 = 0.2562$; *npr1-1*: $y = -0.0579x^2 + 2.26x + 1.673$, $P = 0.0001$, adjusted $R^2 = 0.161$.

Plant defense phytohormone networks, like SA and JA, help shape the immune responses of a plant host while also shape the virulence gene expression within bacterial pathogens, such as *Pseudomonas syringae* (Nobori et al., 2018). To test how variation in host SA/JA-signaling influences the fungal pathogen transcriptome, we applied a generalized linear model linked with negative-binomial function (nbGLM) to each *B. cinerea* transcript across the experiment. This analysis allowed us to estimate the relative broad-sense heritability (H^2) of genetic variation from

185 the pathogen, plant host, or their interaction contributing to each transcript. Of the 9,284
186 detectable *B. cinerea* transcripts, 8,603 and 5,244 transcripts were significantly influenced by
187 genetic variation in pathogen and host, respectively (74% and 45% of predicted *B. cinerea* gene
188 models, respectively) (Figure 2A, Supplemental Data Set 3 and 5). While this result shows that
189 the plant phytohormone pathways influence *B. cinerea* gene expression, the variation in host
190 defense responses (average $H^2_{\text{Host}} = 0.010$) has far less influence on *B. cinerea* gene expression
191 than that of the pathogens' own natural genetic variation (average $H^2_{\text{Isolate}} = 0.152$). The host
192 defense hormones also affected *B. cinerea* gene expression in a genotype-by-genotype dependent
193 manner on 4,541 genes (39% of *B. cinerea* predicted gene models, average $H^2_{\text{Isolate x Host}} = 0.116$)
194 (Figure 2B-2I). Thus, pathogen natural genetic variation has a larger impact on pathogen
195 transcriptional responses *in planta* than variation in host defense responses.

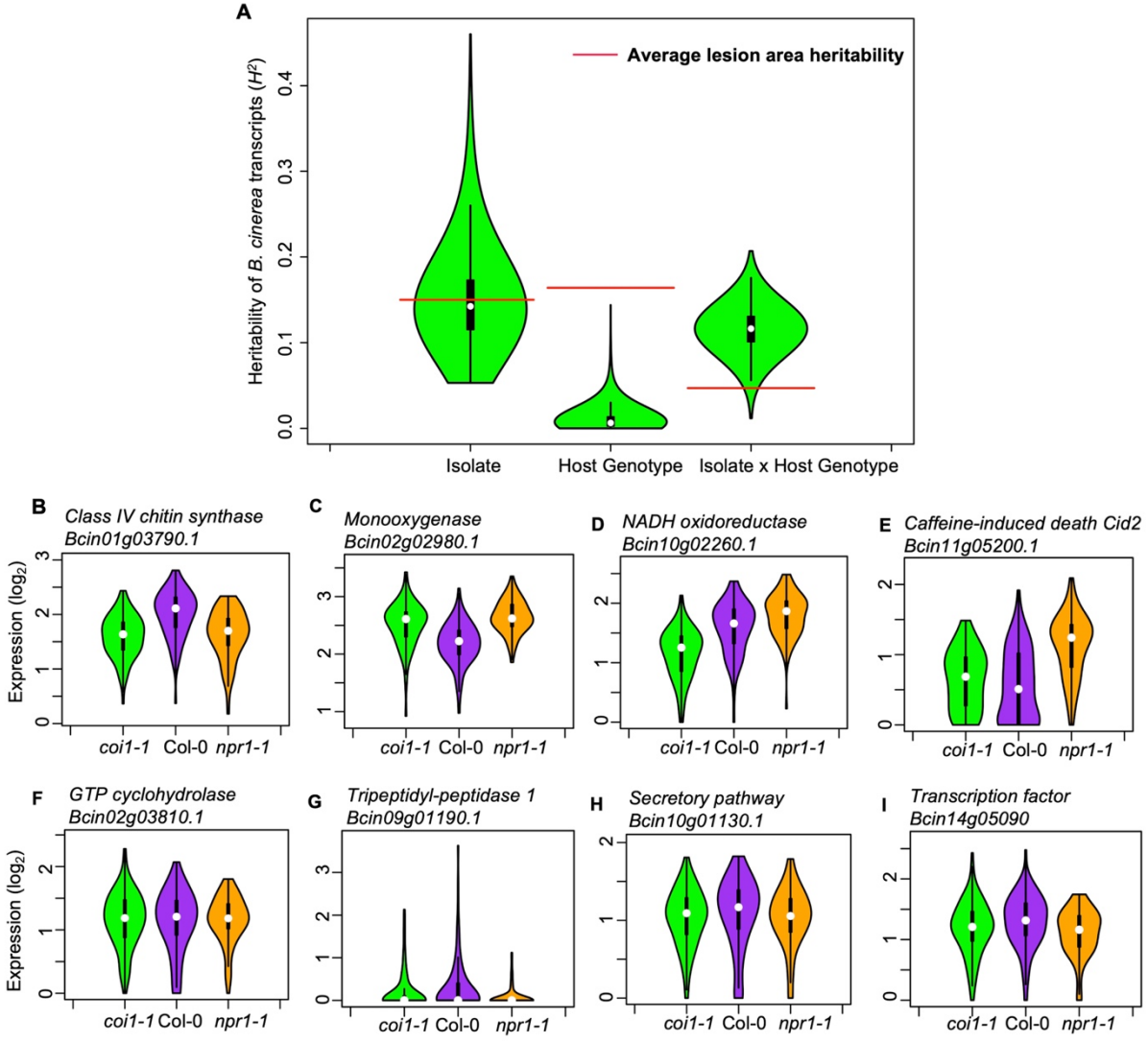

Figure 2. Transcriptomic responses of *B. cinerea* on Arabidopsis are controlled by genetic variation in pathogen population, host genotypes, and their interaction. (A) Distribution of broad-sense heritability (H^2) of *B. cinerea* transcripts contributed by genetic variation in the *B. cinerea*, Arabidopsis genotypes, and the interaction between pathogen and host. Violin plots illustrating the distribution of H^2 for transcripts from 96 *B. cinerea* isolates infecting on Arabidopsis genotypes. Heritability is partitioned across the different sources, 96 pathogen genotypes = "Isolate", plant genotypes Col-0, *coi1-1* and *npr1-1* plant genotypes = "Host", and the corresponding interaction. The transcriptomic analysis was conducted by sequencing mRNA extracted from *B. cinerea* infected Arabidopsis leaves at 16-hours post-infection. Red lines indicate the average broad-sense heritability values of lesion area caused by isolates, Arabidopsis genotypes, and their interaction. (B) to (E) Expression profiles of *B. cinerea* transcripts significantly influenced by host genotypes. The model-corrected means (log_2) for *B. cinerea* transcript were used for plotting. The Arabidopsis genotypes, wild-type Col-0 (purple), jasmonate insensitive mutant *coi1-1* (green), and salicylic acid mutant *npr1-1* (orange), are shown on the x axis. *B. cinerea* transcripts are: (B) *Bcin01g03790.1*, class IV chitin synthase; (C) *Bcin02g02980.1*, Monooxygenase; (D) *Bcin10g02260.1*, NADH oxidoreductase; (E) *Bcin11g05200.1*, caffeine-induced death Cid2; (F) to (I) Expression profiles of *B. cinerea* transcripts significantly influenced by the interaction between pathogen and host genotypes. (F) *Bcin02g03810.1*, GTP cyclohydrolase; (G) *Bcin09g01190.1*, Tripeptidyl-peptidase 1; (H) *Bcin10g01130.1*, in secretory pathway; (I) *Bcin14g05090.1*, a transcription factor.

196

Identification of Virulence Factors Among the Early *B. cinerea* Transcripts

This data set also allows us to test for specific *B. cinerea* transcripts whose early expression is associated with later lesion development. These genes can serve as potential biomarkers of overall pathogen virulence and may elucidate the functional mechanisms driving early virulence in the interaction. To find individual pathogen transcripts link with lesion development, we conducted a genome-wide false discovery rate-corrected Spearman's rank correlation analysis between 72 HPI lesion area and individual *B. cinerea* transcripts accumulation at 16 HPI. We identified 2,521 genes (22% of *B. cinerea* predicted gene models) with significant positive correlations and 114 genes (1% of *B. cinerea* predicted gene models) with significant negative correlations to lesion area across three Arabidopsis genotypes, respectively (P-value < 0.01, Supplemental Data Set 6). The top 20 positively correlated *B. cinerea* genes contained all seven genes involved in BOT biosynthesis (Deighton et al., 2001; Colmenares et al., 2002; Wang et al., 2009; Rossi et al., 2011; Ascari et al., 2013; Porquier et al., 2016). In addition to phytotoxins, more than 30 genes of the top 100 lesion-correlated genes encode plant cell wall degrading enzymes, i.e., glucosyl hydrolases, carbohydrate esterases, cellobiose dehydrogenases and polygalacturonase (Supplemental Data Set 6) (Gerbi et al., 1996; Zamocky et al., 2006; Cantarel et al., 2009; Van Vu et al., 2012; Igarashi et al., 2014; Ingo Morgenstern et al., 2014; Blanco-Ulate et al., 2014; Tien-chye Tan et al., 2015; Courtade et al., 2016; Nelson et al., 2017; Pérez-Izquierdo et al., 2017). For example, the gene encoding the well-studied polygalacturonase 1 (*Bcpg1*) showed a dramatic expression variation across 96 isolates under different host immunities (Figure 3 and Supplemental Data Set 1). Additional 10 of the top 100 lesion-correlated genes were annotated encoding putative peptidase activities, which are critical for fungal virulence (Movahedi et al., 1991; Poussereau et al., 2001; ten Have et al., 2004; ten Have et al., 2010). A final classical virulence gene in the top 100 gene list is *Bcoah* (*Bcin12g01020*) encoding oxaloacetate acetyl hydrolase, which is a key enzyme in oxalic acid biosynthesis and positively contributes to virulence (Supplemental Figure 1 and Supplemental Data Set 6) (Greenberg et al., 1994; Williamson et al., 2007; Walz et al., 2008; Schumacher et al., 2012; Schumacher et al., 2015; Tayal et al., 2017). In addition, this method identified 37 of the top 100 lesion-correlated genes with no gene ontology (GO) terms, which likely represent unknown virulence mechanisms (Supplemental Data Set 6). Thus, this approach readily identifies known and novel pathogen virulence functions.

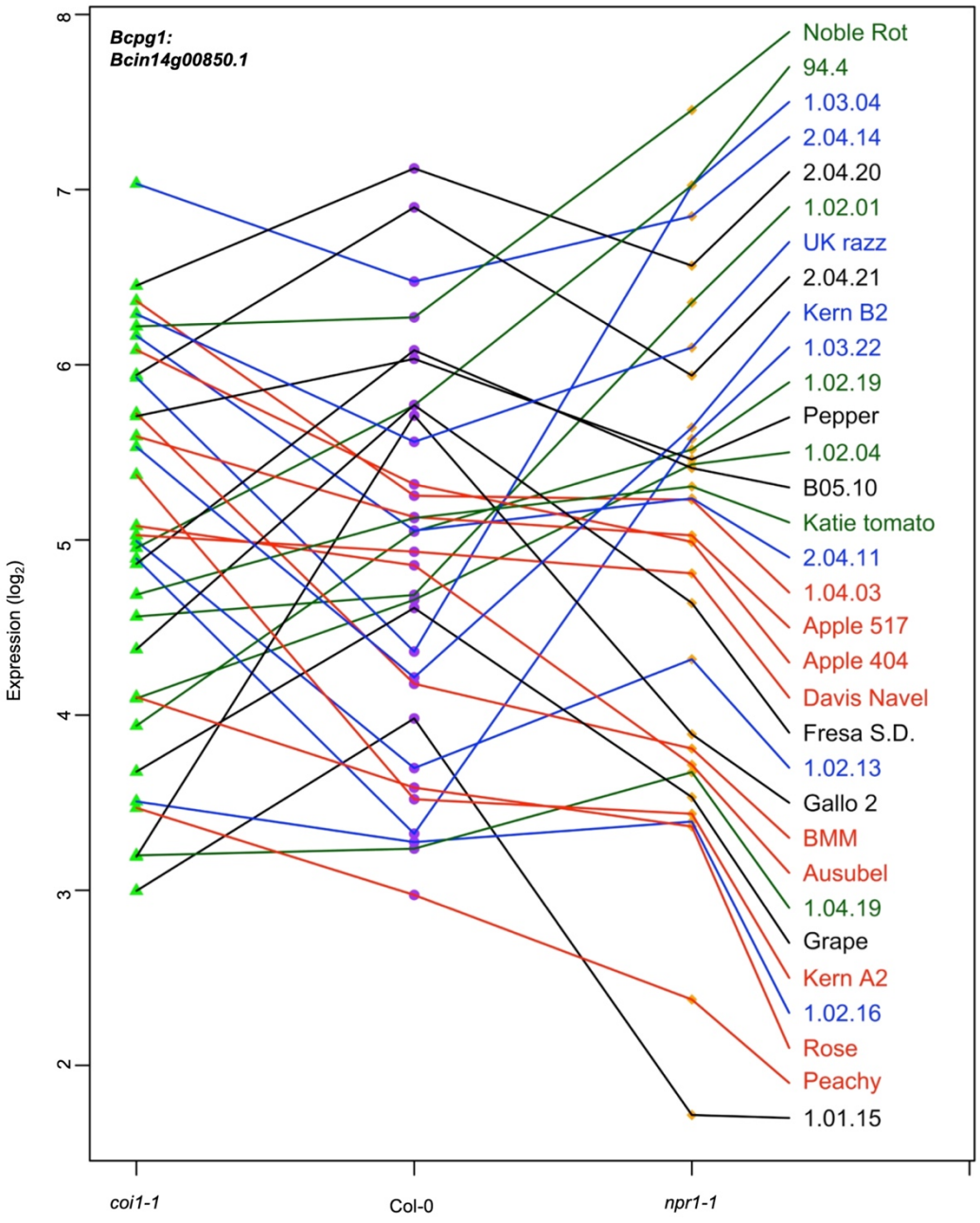

Figure 3. Expression profiles of an endopolygalacturonase gene *Bcpg1* from diverse *B. cinerea* isolates across Arabidopsis genotypes. Rank plot shows the relationship of *Bcpg1* expression from 32 diverse *B. cinerea* isolates (right) across three Arabidopsis genotypes (x axis). Three Arabidopsis genotypes are wild-type Col-0 (purple dot), jasmonate insensitive mutant *coi1-1* (green triangle), and salicylic acid mutant *npr1-1* (orange diamond). The model-corrected means (log_2) for the transcript of *Bcpg1* (*Bcin14g00850.1*) encoding an endopolygalacturonase gene are utilized for plotting. The transcript expression levels from the same isolate across three Arabidopsis genotypes are connected with a colored line. The names of 32 isolates are represented with the same colored lines as induced *Bcpg1* expression levels. Black lines indicate the expression levels of *Bcpg1* are higher in *coi1-1* and *npr1-1* than in Col-0. Red lines indicate the higher expression levels of *Bcpg1* in *coi1-1* but lower in *npr1-1*. Blue lines indicate the highest expression levels of *Bcpg1* are in Col-0. Dark green lines indicate the higher expression levels of *Bcpg1* in *npr1-1* but lower in *coi1-1*.

228

In Planta Virulence Gene Co-expression Networks (GCNs) in *B. cinerea*

To develop a systemic view of fungal pathogen *in planta* gene expression, we used a co-expression approach to identify *B. cinerea* networks that associated with growth and virulence *in planta*. Using solely *B. cinerea* transcriptome at 16 HPI from Arabidopsis Col-0 WT infected leaves, we calculated Spearman's rank correlations of gene counts across all *B. cinerea* isolates, filtered gene pairs with correlation greater than 0.8. We then used the filtered gene pairs as input to construct GCNs. We identified ten distinct GCNs containing more than five *B. cinerea* genes (Figure 4, Supplemental Table 1, Supplemental Figure 2 and Supplemental Data Set 7). The largest GCN with 242 genes contains members responsible for phospholipid synthesis, eiosome function, and membrane-associated stress signaling pathways (Figure 4-Vesicle/virulence). The biological function of this GCN suggests its role in fungal membrane- and vesicle-localized processes, which are normally involved with general hyphae growth, fungal cell wall deposition, and exudation of fungal toxins to the intercellular space (Supplemental Data Set 7). The second largest network contains 128 genes that were entirely associated with translation and protein synthesis (Figure 4-Translation/growth and Supplemental Data Set 7). Of the smaller GCNs identified (5-20 genes), five networks were identified with genes distributed across *B. cinerea* 16 chromosomes, suggesting that these GCNs arise from coordinated trans-regulation (Figure 4-Trans-networks and Supplemental Figure 3D, 3F, 3H-3G). These networks are associated with diverse array of virulence functions, including the regulation of exocytosis, copper transport, the production of peptidases and isoprenoid precursors (IPP), and polyketide secretion.

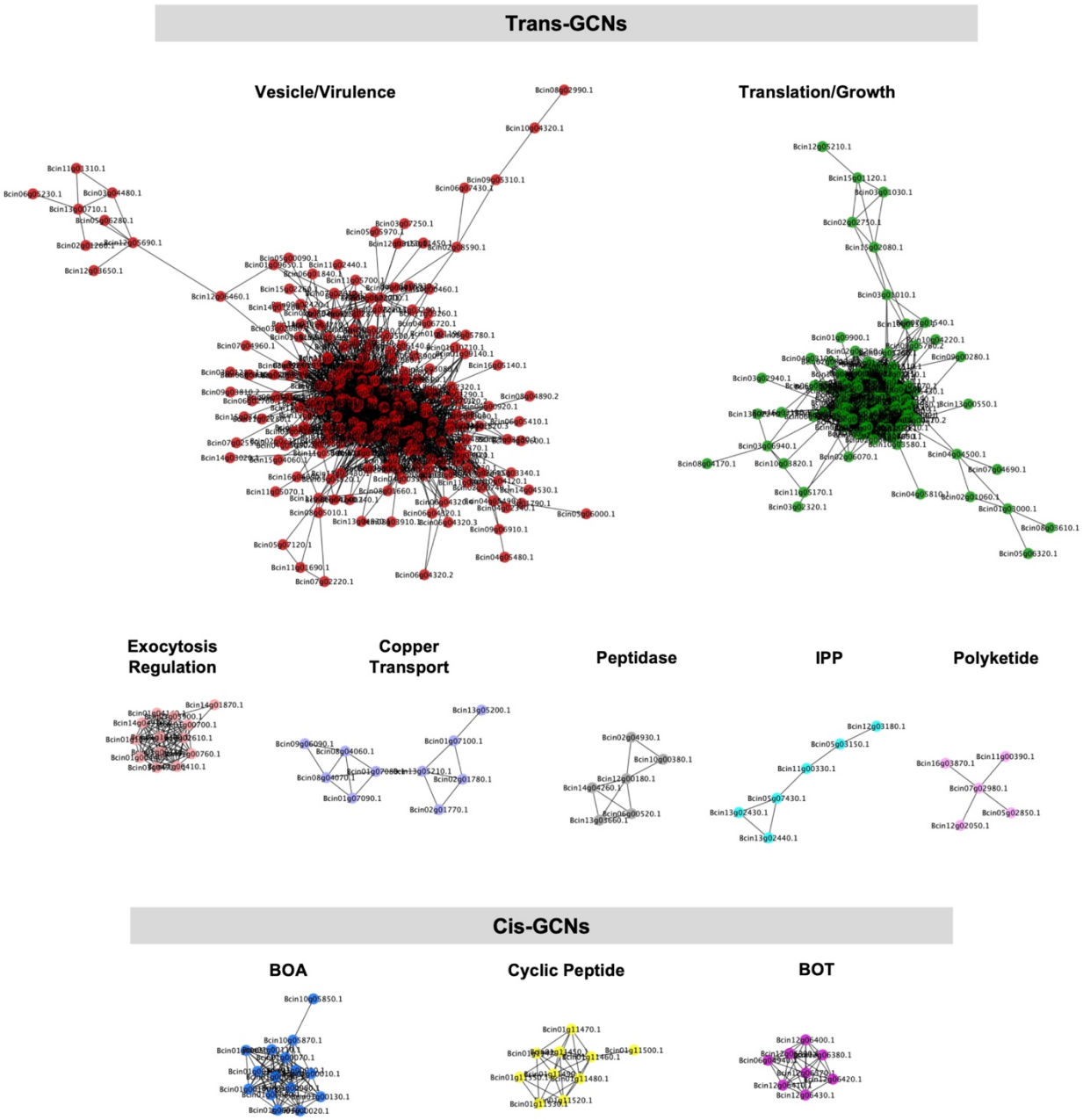

Figure 4. Gene co-expression networks identified from *B. cinerea* transcriptomic responses to Arabidopsis wild-type Col-0 immunity. Ten gene co-expression networks (GCNs) with more than five nodes were identified from 96 *B. cinerea* isolates infecting on Arabidopsis wild-type Col-0. The similarity matrix is computed using Spearman's rank correlation coefficient. Nodes with different colors represent *B. cinerea* genes condensed in GCNs with different biological functions. Edges represent the Spearman's rank correlation coefficients between gene pairs. Trans- and cis-GCNs means GCNs are regulated by trans- and cis-regulatory elements, respectively. GCNs were named after their biological functions, which were determined by hub and bottleneck genes within each network. GCNs are: vesicle/virulence (red), translation/growth (green), exocytosis regulation (pink), cyclic peptide (yellow), peptidase (gray), isopentenyl pyrophosphate (IPP, turquoise), polyketide (violet), botcinic acid (BOA, blue), copper transport (slate blue), botrydial (BOT, purple).

249

In contrast to the whole-genome distributed GCNs, three of the smaller GCNs were comprised of genes tandemly clustered within a single chromosome (Figure 4-BOA, -Cyclic Peptide, -BOT, Supplemental Figure 3C, 3E, and 3G). A functional analysis showed that all of the genes within these networks encoded known or putative biosynthetic enzymes for specialized metabolic pathways. For example, seven genes responsible for BOT biosynthesis cluster on chromosome 12 and form a small GCN with a Zn(II)2Cys6 transcription factor that is specific to the pathway (Figure 5A, 5B, Supplemental Figure 3G and Supplemental Data Set 7) (Siewers et al., 2005; Pinedo et al., 2008; Urlacher and Girhard, 2012; Moraga et al., 2016). Similarly, all 13 genes involved in BOA biosynthesis cluster in Chromosome 1 and form a highly connected GCN (Figure 4-BOA, Figure 5E, Supplemental Figure 3C and Supplemental Data Set 7) (Dalmais et al., 2011). In addition to previously characterized secondary metabolic pathways, we identified an uncharacterized set of ten genes that cluster on Chromosome 1 (Figure 4-Cyclic Peptide, Figure 5F, Supplemental Figure 3E and Supplemental Data Set 7). These genes share considerable homology with enzymes related to cyclic peptide biosynthesis and may represent a novel secondary metabolic pathway in *B. cinerea* (Supplemental Data Set 7). The expression of these pathways *in planta* was extremely variable among the isolates and included some apparent natural knockouts in the expression of the entire biosynthetic pathway (Figure 5G and Supplemental Data Set 1). Isolate 94.4 was the sole genotype lacking the entire BOT pathway, while 19 isolates and 24 isolates did not transcribe the respective BOA and the putative cyclic peptide pathways (Figure 5E to 5G and Supplemental Data Set 1). We decomposed the expression of these pathways into expression vectors, referred to as eigengenes, using a principle component analysis and used a linear mixed model to test for a relationship between early expression of secondary metabolic pathways and later lesion area. This showed a significant relationship between the expression of BOT and BOA pathways and later lesion area (Supplemental Table 2). In contrast, the putative cyclic peptide pathway was only associated with lesion development in a BOT-dependent manner, suggesting that it may have a synergism to BOT (Supplemental Table 2). Thus, *in planta* analysis of the fungal transcriptome can identify known and novel potential virulence mechanisms and associate them with the resulting virulence.

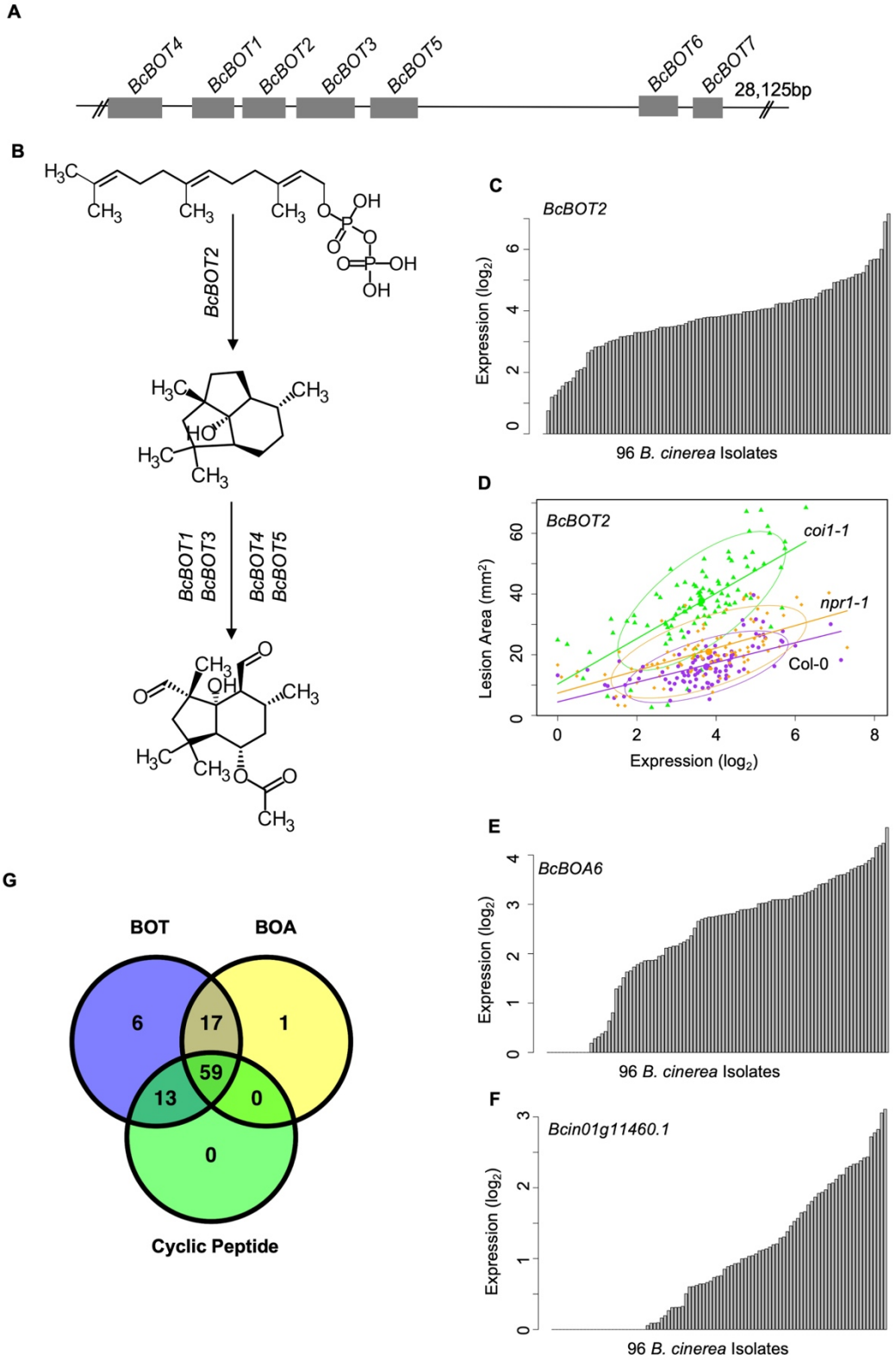

279

Figure 5. Variation of transcripts accumulation for secondary metabolites production across diverse *B. cinerea* isolates. Expression profiles of genes responsible for botrydial, botcinic acid, cyclic peptide production across 96 isolates under Arabidopsis wild-type Col-0 are shown. **(**A) Schematic shows the genomic locus of seven botrydial (BOT) biosynthesis genes clustered together. Exons are represented by gray boxes. Introns and intergenic regions are represented by the grey line. Seven BOT genes are: *BcBOT1, BcBOT3* and *BcBOT4,* encoding a cytochrome P450 monooxygenase, respectively; *BcBOT2* encoding a sesquiterpene cyclase; *BcBOT5* encoding an acetyl transferase; *BcBOT6* encoding a Zn(II)2Cys6 transcription factor, *BcBOT7* encoding a dehydrogenase reductase. (B) BOT biosynthesis pathway in *B. cinerea*. (C) Bar plots compare expression variation of *BcBOT2* across 96 *B. cinerea* isolates in responding to Arabidopsis wild-type Col-0 immunity. The model-corrected means (log_2) of transcripts were used for plotting. (D) Scatter plot illustrates the positive correlations between lesion area and accumulation of *BcBOT2* transcript across the 96 isolates in response to varied Arabidopsis immunities. Model-corrected lesion area means were estimated for three Arabidopsis genotypes at 72-hours post-infection with 96 *B. cinerea* isolates. The three Arabidopsis genotypes are labeled next to the confidence ellipse curves: wild-type Col-0 (purple dot), jasmonate insensitive mutant *coi1-1* (green triangle), and salicylic acid mutant *npr1-1* (orange diamond). The 90% confidence ellipse intervals are plotted for each Arabidopsis genotype for reference. Linear regression lines: Col-0: y = 3.2532x + 4.4323, *P* = 1.008e-10, Adjusted R^2 = 3.3537; *coi1-1*: y = 7.4802x + 10.3289, *P* = 7.895e-15, adjusted R^2 = 0.4700; *npr1-1*: y = 3.7086x + 7.3487, *P* = 2.425e-11, adjusted R^2 = 0.3726. (E) and (F) Bar plots compare expression variation of *BcBOA6* in botcinic acid (BOA) pathway and *Bcin01g11460.* in cyclic peptide pathway across 96 *B. cinerea* isolates in response to Arabidopsis wild-type Col-0 immunity. (G) Venn diagram illustrates the number of *B. cinerea* isolates with the ability to induce BOT, BOA, and cyclic peptide.

Covariation of Fungal Virulence Networks Under Differing Plant Immune Responses

The *B. cinerea* GCNs measured within Arabidopsis WT provide a reference to investigate how phytohormone-signaling in host innate immunity may shape the pathogen's transcriptional responses during infection. Comparing the *B. cinerea* GCN membership and structure across the three Arabidopsis genotypes (WT, *coi1-1*, and *npr1-1*) showed that the core membership within networks was largely maintained but the specific linkages within and between GCNs were often variable (Figure 6, Supplemental Table 1, Supplemental Figure 2, 4 and 5, and Supplemental Data Set 7). For example, the two largest *B. cinerea* GCNs in WT developed multiple co-expression connections during infection in the JA-compromised *coi1-1* host. In the SA-compromised *npr1-1*, however, these GCNs maintained their partition but the membership within each GCN shrunk (Figure 6 and Supplemental Table 1). In contrast, some GCNs are highly robust in both gene content and topology structure across three host genotypes, including three GCNs associated with BOT, BOA and cyclic peptide production, and GCNs associated with exocytosis regulation, copper transport, and peptidase activity (Supplemental Table 1, Supplemental Figure 2, 4 and 5, and Supplemental Data Set 7). In addition, we also identified additional small GCNs that demonstrated host specificity in *coi1-1* (Supplemental Figure 4 and Supplemental Data Set 7). In particular, there were four small GCNs that are associated with plant cell wall degradation, siderophores, glycolysis, ROS, and S-adenosylmethionine biosynthesis. Thus, the coordinated transcriptional responses of *B. cinerea* GCNs are at least partially dependent on variation in the host immune response.

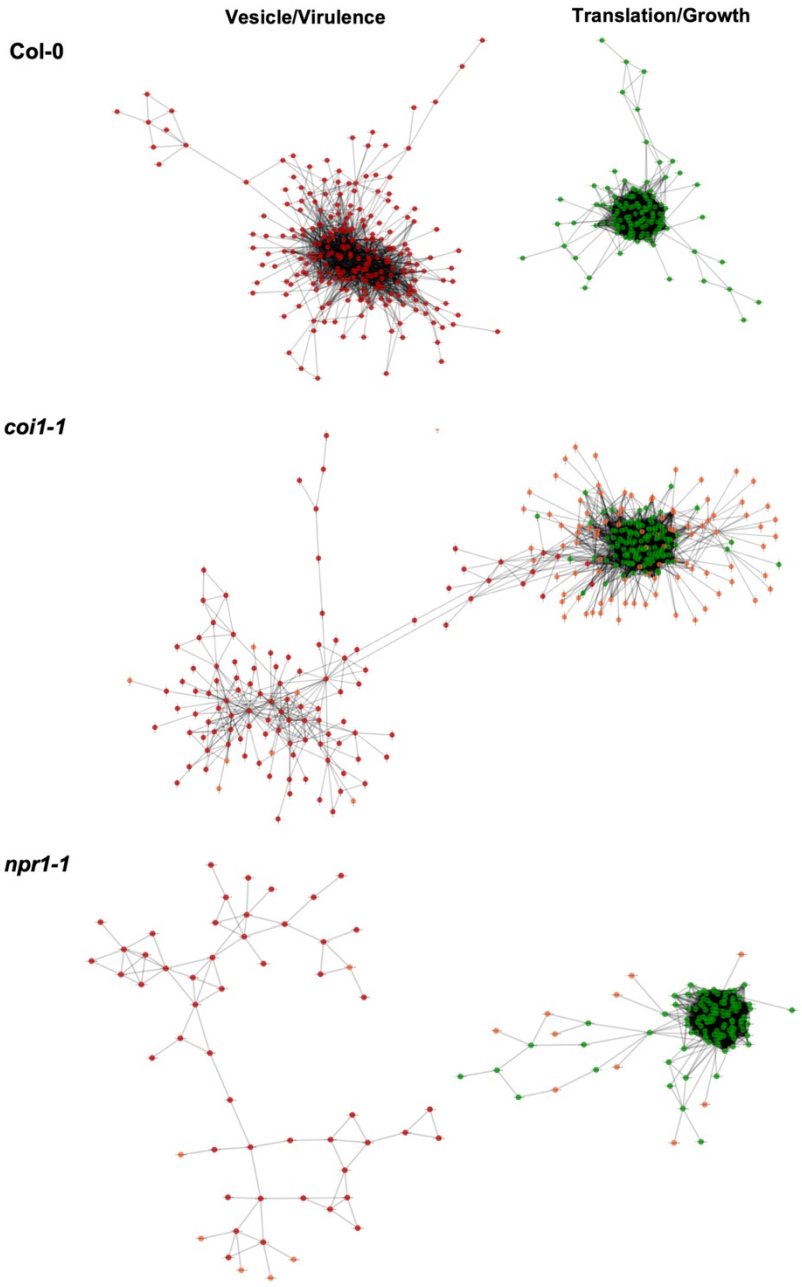

Figure 6. Comparison of plasticity of *B. cinerea* gene co-expression network under vaired host immunity. *B. cinerea* gene co-expression networks (GCNs) of vesicle/virulence (red) and translation/growth (green) identified under three Arabidopsis genotypes are compared. Three Arabidopsis genotypes are wild-type Col-0, jasmonate insensitive mutant *coi1-1*, and salicylic acid mutant *npr1-1*. Nodes marked with red and green colors represent *B. cinerea* genes condensed in GCNs with different biological functions. The same node condensed in GCNs across three Arabidopsis genotypes was marked with same color. Nodes specificaly condensed in GCNs under two mutants *coi1-1* and *npr1-1* background are marked with orange color. Edges represent the Spearman's rank correlation coefficients between gene pairs.

Host immunities showed different impacts on expression profiles of genes condensed in individual *B. cinerea* GCNs (Supplemental Figure 6). Compared with WT, expression profiles of genes within the largest membrane/vesicle virulence GCN were elevated in the SA- and JA-compromised Arabidopsis mutants on average (Supplemental Figure 6A). Fungal genes associated with copper transport and polyketide production were upregulated under SA-compromised host immunity (Supplemental Figure 6F and 6J). Whereas, members of GCNs responsible for plant cell wall degradation and siderophore biosynthesis were upregulated under JA-compromised host immunity (Supplemental Figure 6K and 6L). Finally, GCNs associated with BOT and exocytosis regulation showed robust gene expression profiles across all three Arabidopsis genotypes (Supplemental Figure 6D and 6G). The above observation indicates host immunity influences the *B. cinerea* transcriptional response of *B. cinerea* and suggests that *B. cinerea* isolates have varied abilities to tailor virulence strategy in response to host immunity.

A Dual Interaction Network Reveals Fungal Virulence Components Targeting Host Immunity

To begin assessing how two species influence each other's gene expression during infection, we constructed a co-transcriptome network using both host- and pathogen-derived GCNs. We converted the ten *B. cinerea* GCNs and the four Arabidopsis GCNs into eigengene vectors that capture the variation of the general expression of all genes within a GCN into a single value (Zhang et al., 2017). We calculated Spearman's rank coefficients among each GCN eigengene pairs without regard for the species. In this dual transcriptome network, the Arabidopsis/*B. cinerea* GCN eigengenes are displayed as nodes and positive/negative correlations between the GCNs as edges (Figure 7). Of the host-derived GCNs, the Arabidopsis Defense/camalexin and Photosystem I (PSI) GCNs have a higher degree of centrality within the dual interaction network, suggesting that they have the most interactions with *B. cinerea* GCNs. The fungal GCNs highest degrees were associated with the exocytosis regulation, BOT, and IPP, which further illustrating the importance of specialized metabolism exudation in pathogen virulence. Interestingly, fungal GCNs (copper transport, exocytosis regulation, BOT and IPP biosynthesis) that were positively correlated with the host Defense/camalexin GCN showed negative correlations with PSI eigengene. The opposite correlationships between pathogen- and host-GCNs suggest that these fungal GCNs may target plant PSI while the plant counters this attack using the Defense/camalexin GCN. To test if these connections were dependent upon the host

immunity, we used the eigengene values derived from fungal GCNs to conduct mixed linear modelling of how they were linked to variation in the host genotype and/or host GCNs (Supplemental Table 3 and 4). Some *B. cinerea* GCNs (Vesicle/virulence and TSL/growth, etc.) were affected by variation in the host genotypes but others showed host-independent manner (BOT, copper transport, etc.). Critically, the connections between pathogen- and host-GCNs were largely independent of the host genotypes, suggesting that the dual interaction network is a relatively robust structure (Supplemental Table 3 and 4). Collectively, pathogen virulence and host immunity GCNs showed complex connections within dual interaction network identified from co-transcriptome data, suggesting functional relationships between host defense and pathogen virulence mechanisms for future experimentation.

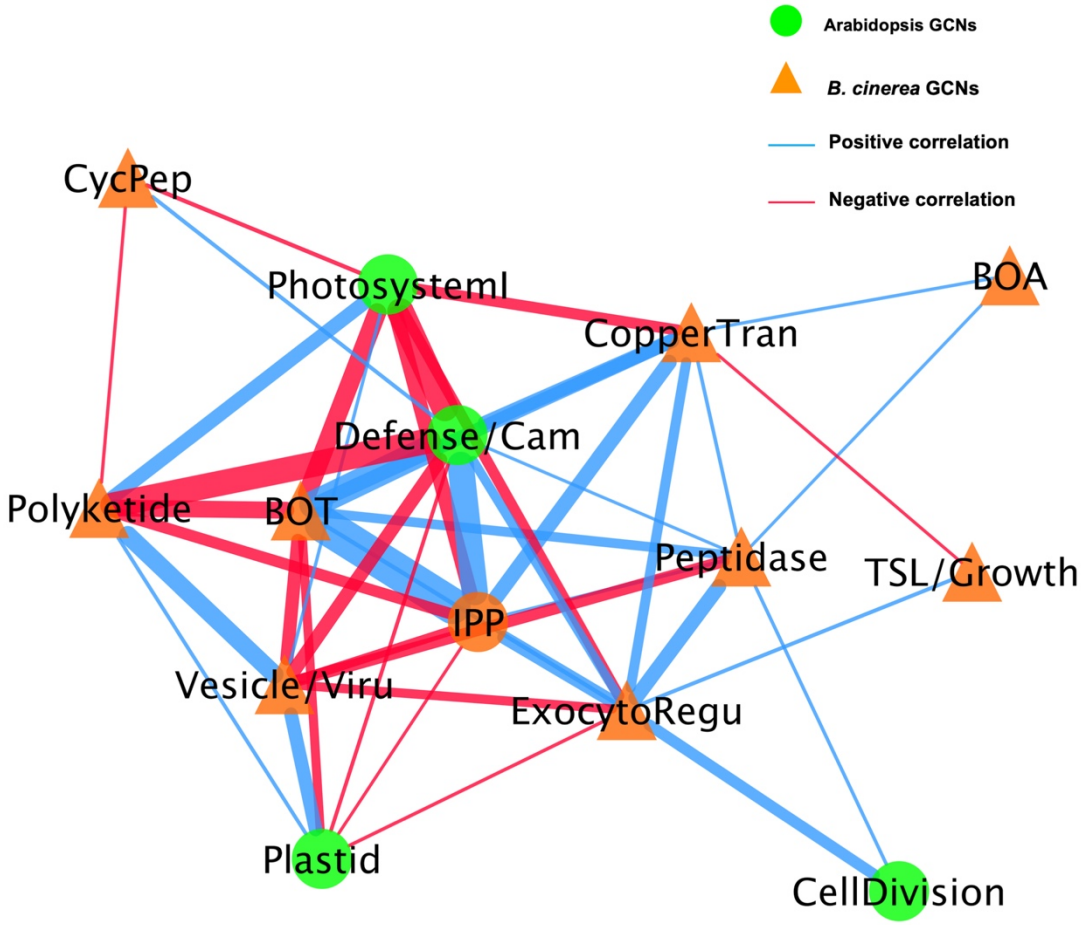

Figure 7. A dual interaction network reveals links between Arabidopsis immunity and *B. cinerea* virulence. A dual interaction network was constructed using gene co-expression networks (GCNs) from Arabidopsis and *B. cinerea* co-transcriptome. The first eigenvectors were derived from individual GCNs and used as input to calculate Spearman's rank correlation coefficiency between GCN pairs. Green dots and orange triangles represent Arabidopsis immune- and *B. cinerea* virulence-GCNs, respectively. Blue and red lines (edges) represent the positive and negative Spearman's rank correlation coefficients between GCN pairs, respectively. The thickness of line signifies the correlational strength.

343

344 To test the direct interaction between individual genes from two organisms, we conducted
345 Arabidopsis-*B. cinerea* GCNs using co-transcriptome data under each host genotype. We
346 calculated Spearman's rank correlation coefficients among 23,898 Arabidopsis transcripts and
347 9,284 *B. cinerea* transcripts. This approach allowed us to identify three cross-kingdom GCNs

(CKGCNs) under Arabidopsis WT and JA- or SA-compromised two mutants (Supplemental Figure 7, Supplemental Table 5, and Supplemental Data Set 8). Under Arabidopsis WT, a total of 54 hub genes were identified and half of them from the *B. cinerea* genome. Furthermore, CKGCNs contain a majority of genes in the BOT GCN and a small proportion of genes in the vesicle/virulence GCN (Supplemental Figure 8G, 8F, and 8H). For plants, CKGCNs contain a majority of genes from Arabidopsis Defense/camalexin GCN (Supplemental Figure 8C, 8D, and 8F). These CKGCNs also contain genes associated with extensive host defense responses, i.e., genes encoding membrane-localized leucine-rich repeat receptor kinases (LRR-RKs), stress signal sensing and transduction, tryptophan-derived phytoalexin production, regulation of cell death, cell wall integrity, nutrition transporters, etc. (Supplemental Data Set 8). CKGCNs varied their topological structure and gene content across the three Arabidopsis genotypes (Supplemental Figure 7). Shifting of core gene set and hub genes across host genotypes indicate the important role of virulence and immunity provided by individual genes depending on the host-pathogen interaction.

DISCUSSION

In recent decades, improved understanding of the molecular basis of plant-pathogen dynamics has facilitated breeding strategies for disease resistance in a variety of crop species. However, breeding for disease resistance remains difficult for crops susceptible to pathogens that harbor diverse polygenic virulence strategies targeting multiple layers and components of the plant innate immune system (Corwin and Kliebenstein, 2017). In this study, we investigated the transcriptome profiles at an early infection stage both within *B. cinerea* and across the interaction within the Arabidopsis-*B. cinerea* pathosystem. This showed that the transcriptional virulence strategy employed by *B. cinerea* is dependent both on fungal genotype and the functional response of the host plant's immune system. We identified a batch of early *B. cinerea* transcripts associated with later lesion development and several pathogen GCNs responsible for mediating virulence in *B. cinerea*, including a potential specialized metabolic pathway of cyclic peptide virulence factor. Lastly, we constructed a co-transcriptome network that revealed known and novel fungal virulence components coordinated expressed with plant host GCNs during infection.

Secondary Metabolites Mediate Plant and Fungus Transcriptomic Interactions During Infection

Necrotrophic pathogen *B. cinerea* has evolved an arsenal of virulence strategies to establish colonization and enhance infection within the plant host, including production of secondary metabolites. The co-transcriptome approach shows that the expression of fungal specialized pathways early in infection correlates with later lesion development (Supplemental Table 3). Three secondary metabolite GCNs are clustered within the fungal genome and two of them identified with pathway-specific transcription factors (Figure 5, Supplemental Figure 4 and Supplemental Data Set 7). Further, the expression of these pathways displayed a large range of phenotypic variation across the isolates (Figure 5G and Supplemental Data Set 1). However, the topology and memberships of GCNs for the three pathways are largely insensitive to variation in host immunity. Robustness to host immunity suggests that these GCNs are somehow insulated from the host's immune response, possibly to protect toxin production from a host counter-attack. The co-transcriptome approach showed the ability to identify known and novel secondary metabolic pathways that mediate plant host and fungal pathogen interaction.

Importantly, dual interaction network indicated pathogen-GCNs responsible for fungal secondary metabolites production link to specific plant host-GCNs (Figure 7). Specifically, the co-transcriptome approach revealed that *B. cinerea* GCNs responsible for secondary metabolite production are positively associated with plant immune responses and negatively associated with primary plant metabolism (Figure 7, Supplemental Table 3 and 4). For example, the BOT GCN shows a strong positive correlation with the Arabidopsis defense/camalexin GCN, suggesting that BOT production may directly induce the host's defense system. Concurrently, the BOT GCN is negatively linked to the plant's PSI GCN, suggesting that BOT may repress the plant's photosynthetic potential. Further work is needed to test the direction of causality within the dual interaction network as it is possible that the host's defense/camalexin network is responding to the PSI alteration, or vice versa. Collectively, these results strongly implicate the ability of secondary metabolites biosynthesis to mediate the interactions between pathogen virulence and plant host immunity at the transcriptomic level. The co-transcriptome approach showed the potential to enable us to form new hypotheses about how this linkage may occur.

Fungal Virulence Components Correlated with Plant Immune Response

In addition to secondary metabolite biosynthesis, the co-transcriptome identified a number of key virulence mechanisms that could be mapped to the two species interaction. One key GCN is enriched for genes involved in exocytosis associated regulation (Figure 4-exocytosis regulation and Supplemental Data Set 7). The exocytosis complex is responsible for delivery of secondary metabolites and proteins to the extra-cellular space and plasma membrane in fungi (Colombo et al., 2014; Rodrigues et al., 2015). Additionally, we found many *B. cinerea* genes associated with secretory vesicles within the membrane/vesicle virulence GCN that likely serve a similar function during infection (Figure 4-Vesicle/virulence and Supplemental Data Set 7). These GCNs also provide support for the role of exocytosis-based spatial segregation of different materials during fungal hyphae growth *in planta* (Samuel et al., 2015). The dual interaction network suggests that the exocytosis regulation and membrane/vesicle virulence GCNs are differentially linked to the Arabidopsis defense/camalexin GCN, indicating varied connections between fungal secretory pathways and plant immune responses (Figure 7 and Supplemental Table 3 and 4). Another conserved GCN in the *B. cinerea* species is associated with copper uptake and transport (Figure 4-Copper transport, Supplemental Figure 2, 4, 5, and Supplemental Data Set 7). Although copper is essential for *B. cinerea* penetration and redox status regulation within plant tissues, further work is required to decipher the precise molecular mechanism involved in acquisition and detoxification of copper. Thus, the co-transcriptome approach can identify both known and unknown mechanisms and links within the host-pathogen interaction.

Fungal Virulence Transcriptomic Responses Are Partly Shaped by Host Immunity

It is largely unknown how plant host immunity contributes to the transcriptomic behavior of the fungus during infection. Even less is known about the role of genetic variation in the pathogen in responding to, or coping with, the inputs coming from the host immune system. In the current study, we found that the host immune system was able to alter the expression of only some of pathogen transcripts and GCNs (Figure 2, Figure 6, Supplemental Figure 6, and Supplemental Data 5). For example, fungal GCNs associated with membrane/vesicle virulence and fungal growth shifted drastically between the WT and *coi1-1* or *npr1-1* Arabidopsis genotypes (Figure 6). In addition, some GCNs only appeared in specific backgrounds. For example, those linked to siderophores and a polyketide production were only identified during infection of the JA-compromised Arabidopsis mutant (Supplemental Figure 6J and 6L). However, other fungal GCNs, like those involved in secondary metabolism, were largely insensitive to variation in the

host immunity (Supplemental Figure 2, 4, 5, Supplemental Table 1, and Supplemental Data Set 7). Critically, the gene membership of these GCNs is largely stable across the collection of pathogen isolates, even while their expression level across the *B. cinerea* isolates is highly polymorphic (Figure 5 and Supplemental Figure 6). This suggests that natural variation in the host immunity and pathogen shapes how the co-transcriptome responds to host's immune system. Further, the natural variation in the pathogen may be focused around these functional GCNs.

Plant Disease Development Can Be Predicted by Early Transcriptome Data

Plant disease development is an abstract phenomenon that is the result of a wide set of spatio-temporal biological processes encoded by two interplaying species under a specific environment. In current study, we used late stage lesion area as a quantitative indicator of *B. cinerea* virulence. We have previously shown that early Arabidopsis transcriptomic response could be linked to later lesion development (Zhang et al., 2017). Here, our findings suggest that the late-stage disease development of a *B. cinerea* infection is determined during the first few hours of infection by the interaction of plant immune and fungal virulence responses. It was possible to create a link between early transcripts' accumulation and late disease development using solely the *B. cinerea* transcriptome (Figure 1 and Supplemental Data Set 6). This could be done using either individual pathogen genes, GCNs, or more simply the total fraction of transcripts from the pathogen. As the transcriptomic data were from plant leaf tissue only 16 HPI, there is not a significant amount of pathogen biomass and this is more likely an indicator of transcriptional activity in the pathogen during infection. It is possible to develop these methods as possible biomarkers for likely fungal pathogen caused disease progression.

CONCLUSION

By analyzing an early stage co-transcriptome of a *B. cinerea* population infection on Arabidopsis, we identified a number of *B. cinerea* GCNs that contained a variety of virulence-associated gene modules with different biological functions. The characterization of these GCNs simultaneously identified mechanisms known to enhance *B. cinerea* virulence and implicated several novel mechanisms not previously described in the Arabidopsis-*B. cinerea* pathosystem. In addition, we characterized a plant-fungus co-transcriptome network and identified the potential interaction between fungal pathogen- and plant host-GCNs. These results shed lights on

468 the biological mechanisms driving quantitative pathogen virulence in *B. cinerea* and their
469 potential targets in the plant innate immune system. This holistic understanding of the plant-
470 pathogen interaction provides an opportunity to better understand and effectively combat crop
471 diseases in agricultural and forest systems.

472 **METHODS**

473 **Collection and Maintenance *B. cinerea* Isolates**

474 A collection of 96 *B. cinerea* isolates were selected in this study based on their phenotypic and
475 genotypic diversity (Denby et al., 2004; Rowe and Kliebenstein, 2007; Corwin, Subedy et al.,
476 2016; Zhang et al., 2016; Zhang et al., 2017). This *B. cinerea* collection was sampled from a
477 large variety of different host origins and contained a set of international isolates obtained from
478 labs across the world, including the well-studied B05.10 isolate. A majority of isolates are
479 natural isolates that isolated from California and can infect a wide range of crops. Isolates are
480 maintained in -80 °C freezer stocks as spores in 20% glycerol and were grown on fresh potato
481 dextrose agar (PDA) 10 days prior to infection.

482 **Plant Materials and Growth Conditions**

483 The Arabidopsis accession Columbia-0 (Col-0) was the wildtype background of all Arabidopsis
484 mutants used in this study. The three Arabidopsis genotypes used in this study included the WT
485 and two well-characterized immunodeficient mutants, *coi1-1* and *npr1-1*, that abolish the major
486 JA- or SA-defense perception pathways, respectively (Cao et al., 1997; Xie et al., 1998; Xu, L.
487 et al., 2002; Pieterse and Van Loon, 2004). All plants were grown as described previously
488 (Zhang et al., 2017). Two independent randomized complete block-designed experiments were
489 conducted and a total of 90 plants per genotype were grown in 30 flats for each experiment.
490 Approximately 5 - 6 fully developed leaves were harvested from the five-week old plants and
491 placed on 1% phytoagar in large plastic flats prior to *B. cinerea* infection.

492 **Inoculation and Sampling**

493 We infected all 96 isolates onto each of the three Arabidopsis genotypes in a random design with
494 6-fold replication across the two independent experiments. A total of twelve infected leaves per

isolate/genotype pair were generated. For inoculation, all *B. cinerea* isolates were cultured and inoculated on three Arabidopsis genotypes as described previously (Denby et al., 2004; Corwin, Copeland et al., 2016; Zhang et al., 2017). Briefly, frozen glycerol stocks of isolate spores were first used for inoculation on a few slices of canned peaches in petri plates. Spores were collected from one-week-old sporulating peach slices. The spore solution was filterred and the spore pellet was re-suspended in sterilized 0.5x organic grape juice (Santa Cruz Organics, Pescadero, CA). Spore concentrations were determined using a hemacytometer and suspensions were diluted to 10 spores/μL. Detached leaf assays were used for a high-throughput analysis of *B. cinerea* infection, which has been shown to be consistent with whole plant assay (Govrin and Levine, 2000; Mengiste et al., 2003; Denby et al., 2004; Sharma et al., 2005; Windram et al., 2012). Five-week old leaves were inoculated with 4 μL of the spore solution. The infected leaf tissues were incubated on 1% phytoagar flats with a humidity dome at room temperature. The inoculation was conducted in a randomized complete block design across the six planting blocks. All inoculations were conducted within one hour of dawn and the light period of the leaves was maintained. Two blocks were harvest at 16 hours post-inoculation (HPI) for RNA-Seq analysis. The remaining four blocks were incubated at room temperature until 72 HPI when they were digitally imaged for lesion size and harvested for chemical analysis as described previously (Zhang et al., 2017).

RNA-Seq Library Preparation, Sequencing, Mapping and Statistical Analysis

Two *B. cinerea* infected leaf tissues of the six blocks were sampled at 16 HPI for transcriptome analysis, which resulted in a total of 1,052 mRNA libraries for Illumina HiSeq sequencing. RNA-Seq libraries were prepared according to a previous method (Kumar et al., 2012) with minor modifications (Zhang et al., 2017). Briefly, infected leaves were immediately frozen in liquid nitrogen and stored at -80 °C until processing. RNA extraction was conducted by re-freezing samples in liquid nitrogen and homogenizing by rapid agitation in a bead beater followed by direct mRNA isolation using the Dynabeads oligo-dT kit. First and second strand cDNA was produced from the mRNA using an Invitrogen Superscript III kit. The resulting cDNA was fragmented, end-repaired, A-tailed and barcoded as previously described. Adapter-ligated fragments were enriched by PCR and size-selected for a mean of 300 base pair (bp) prior to sequencing. Barcoded libraries were pooled in batches of 96 and submitted for a single-end,

50 bp sequencing on a single lane per pool using the Illumina HiSeq 2500 platform at the UC Davis Genome Center (DNA Technologies Core, Davis, CA).

Bioinformatics and Statistical Analysis

Fastq files from individual HiSeq lanes were separated by adapter index into individual RNA-Seq library samples. The quality of individual libraries was estimated for overall read quality and over-represented sequences using FastQC software (Version 0.11.3, www.bioinformatics.babraham.ac.uk/projects/). We conducted downstream bioinformatic analysis, like reads mapping, normalization and nbGLM model analysis, using a custom script from the Octopus R package (https://github.com/WeiZhang317/octopus). The mapping of processed reads against Arabidopsis and *B. cinerea* reference genomes was conducted by Bowtie 1 (V.1.1.2, http://sourceforge.net/projects/bowtie-bio/files/bowtie/1.1.2/) using minimum phred33 quality scores (Langmead et al., 2009). The first 10 bp of reads was trimmed to remove low quality bases using the fastx toolkit (http://hannonlab.cshl.edu/fastx_toolkit/commandline.html). Total reads for each library were firstly mapped against the Arabidopsis TAIR10.25 cDNA reference genome. The remaining un-mapped reads were then aligned against *B. cinerea* B 05.10 isolate cDNA reference genome (Lamesch et al., 2010; Lamesch et al., 2012; Krishnakumar et al., 2015; Van Kan et al., 2017) and the gene counts for both species were pulled from the resulting SAM files (Li et al., 2009).

For pathogen gene expression analysis, we first filtered genes with either more than 30 gene counts in one isolate or 300 gene counts across 96 isolates. We normalized *B. cinerea* gene counts data set using the trimmed mean of M-values method (TMM) from the EdgeR package (V3.12) (Robinson and Smyth, 2008; Bullard et al., 2010; Robinson and Oshlack, 2010). We then ran the following generalized linear model (GLM) with a negative binomial link function from the MASS package for all transcripts using the following equation (Venables and Ripley, 2002):

$$Y_{egai} = E_e + E_e(Gf_g) + E_e(Gf_g(Af_a)) + I_i + H_h + H_h * I_i$$

where the main categorical effects E, I, and H are denoted as experiment, isolate genotype, and plant host genotype, respectively. Nested effects of the growing flat (Gf) within the experimental replicates and agar flat (Af) nested within growing flat are also accounted for within the model.

554 Model corrected means and standard errors for each transcript were determined for each
555 isolate/plant genotype pair using the lsmeans package (Russell V. Lenth, 2016). Raw *P*-values
556 for F- and Chi Square-test were determined using Type II sums of squares using *car* package
557 (Fox and Weisberg, 2011). *P*-values were corrected for multiple testing using a false discovery
558 rate correction (Benjamini and Yekutieli, 2001). Broad-sense heritability (H^2) of individual
559 transcripts was estimated as the proportion of variance attributed to *B. cinerea* genotype,
560 Arabidopsi*s* genotype, or their interaction effects.

561 **_B. cinerea_ Gene Co-expression Network Construction**

562 To obtain a representative subset of *B. cinerea* genes co-expressed under *in planta* conditions,
563 we generated gene co-expression networks (GCNs) among genes in the *B. cinerea* transcriptome.
564 GCNs were generated using the model-corrected means of 9,284 *B. cinerea* transcripts from
565 individual isolate infection across three Arabidopsis genotypes. Only genes with average or
566 medium expression greater than zero across all samples were considered. This preselection
567 process kept 6,372 genes and those with negative expression values were adjusted to set
568 expression at zero before network construction. Spearman's rank correlation coefficients for each
569 gene pair was calculated using the *cor* function in R. Three gene-for-gene correlation similarity
570 matrixes were generated independently for each of the three Arabidopsis genotypes. Considering
571 the cutoff for gene-pair correlation usually generates biases of GCN structure and the candidate
572 gene hit, we utilized several cutoff threshold values at 0.75, 0.8, 0.85, and 0.9 to filter the gene
573 set. Comparing the structure and content of GCNs among those GCN sets using filtered gene set
574 as input, we selected the correlation threshold at 0.8. A total of 600, 700 and 494 *B. cinerea*
575 candidate genes passed the criterion under Arabidopsis WT, mutants *coi1-1* and *npr1-1*,
576 respectively. To obtain a representative subset of *B. cinerea* gene candidates across three host
577 genotypes, we selected gene candidates that presented across the above three gene subsets. This
578 process generated a gene set with 323 *B. cinerea* candidate genes that were common to each of
579 the plant genotype backgrounds and had at least 0.8 significant correlations. Using this gene set
580 as kernel, we extended gene candidate sets under each Arabidopsis genotype. The expanded *B.*
581 *cinerea* gene candidate set under individual Arabidopsis genotypes was further used as input for
582 gene co-expression network construction.

583 GCNs were visualized using Cytoscape V3.2.1 (Java version:1.8.0_60) (Shannon et al., 2003).
584 The nodes and edges within each network represent the *B. cinerea* genes and the Spearman's
585 rank correlations between each gene pair. The importance of a given node within each network
586 was determined by common network analysis indices, such as connectivity (degree) and
587 betweenness. Nodes with higher connectivity and betweenness were considered as hub and
588 bottleneck genes, respectively, and the biological functions of each network were determined by
589 the GO terms of hub and bottle neck genes using Blast2GO.

590 **Dual Interaction Network Construction**

591 To construct a cross-kingdom, dual interaction network of plant-pathogen GCNs, we performed
592 principle component analysis on individual GCNs within each species to obtain eigengene
593 vectors describing the expression of the entire gene network as previously described (Zhang and
594 Horvath, 2005; Langfelder and Horvath, 2008; Okada et al., 2016). From these eigengene
595 vectors, we calculated the Spearman's rank correlation coefficient between the first eigengene
596 vectors for each network. The resulting similarity matrices were used as input to construct the
597 interaction network and Cytoscape was used to visualize the resulting network.

598 **Cross-kingdom Arabidopsis-*B. cinerea* Gene Co-expression Network Construction**

599 We used model-corrected means of transcripts from three Arabidopsis host genotypes and 96 *B.*
600 *cinerea* isolates to construct the cross-kingdom Arabidopsis-*B. cinerea* GCNs. Model-corrected
601 means of 23,959 Arabidopsis transcripts and 6,372 *B. cinerea* transcripts derived from two
602 negative binomial linked generalized linear models were served as input data sets (Zhang et al.,
603 2017). Spearman's rank correlation coefficient was calculated between genes from Arabidopsis
604 and *B. cinerea* data sets. The gene pairs with positive correlations greater than 0.74 under each
605 Arabidopsis genotype were considered to construct cross-kingdom GCNs.

606 **Gene Ontology Analysis**

607 GO analysis was conducted for several *B. cinerea* gene sets that were identified with high
608 heritability, correlated with lesion size, and condensed in network analysis. We first converted
609 sequences of these *B. cinerea* genes into fasta files using Biostrings and seqRFLP packages in R
610 (Ding and Zhang, 2012; Pages et al., 2017). The functional annotation of genes was obtained by

611 blasting the sequences against the NCBI database using Blast2GO to obtain putative GO
612 annotations (Conesa et al., 2005; Gotz et al., 2008). The GO terms were compared to the
613 official GO annotation from the *B. cinerea* database
614 (http://fungi.ensembl.org/Botrytis_cinerea/Info/Index) and those obained by Blast2GO analaysis.
615 The official gene annotations for host genes was retrieved from TAIR10.25
616 (https://apps.araport.org/thalemine/bag.do?subtab=upload).

617 **Statistical Analysis of Network Components**

618 All the analyses were conducted using R V3.2.1 statistical environment (R Core Team, 2014). To
619 investigate how secondary metabolite induction in *B. cinerea* contributes to disease
620 development, we conducted a multi-factor ANOVA on *B. cinerea* three secondary metabolic
621 pathways upon impacts on host genotypes. The three secondary metabolic pathways included the
622 biosynthetic pathways of two well-known secondary metabolites, BOT and BOA, and a cyclic
623 peptide biosynthetic pathway predicted in this study. We calculated the z-scores for all
624 transcripts involved in BOT pathway, the BOA, and the putative cyclic peptide pathway for each
625 isolate/plant genotype pair. The multi-factor ANOVA model for lesion area was:

626 $y_{Lesion} = \mu + T * A * C * G_h + \varepsilon$.

627 where T, A, C, and G_h stand for BOT, BOA, Cyclic peptide, and host genotype, respectively.

628 In addition, we used multi-factor ANOVA models to investigate interactions between GCNs
629 within species for impacts upon host genotypes. The ANOVA models contain all GCNs within a
630 species. The first eigengene vector derived from principal component analysis on each network
631 was used in ANOVA models.

632 The ANOVA model for individual *B. cinerea* GCNs was:

633 $y_{BcNeti} = \mu + D * P * C * PSI * G_h + \varepsilon$

634 where D, P, C, PSI, and G_h stand for Arabidopsis Defense/Camalexin GCN, Arabidopsis Plastid
635 GCN, Arabidopsis Cell/Division GCN, Arabidopsis PSI GCN, and Host genotypes, respectively.
636 G_h stands for HostGenotype, respectively. BcNeti represents one of the ten *B. cinerea* GCNs
637 identified in this study.

The ANOVA model for individual Arabidopsis GCNs was:

$$y_{AtNeti} = \mu + \sum BcNeti + G_h + \varepsilon$$

where ∑BcNeti represents the summation of each of the ten *B. cinerea* GCNs identified in this study: BcVesicle/Viru GCN, BcTSL/Growth GCN, BcBOA GCN, BcExocytoRegu GCN, BcCycPep GCN, BcCopperTran GCN, BcBOT GCN, BcPeptidase GCN, BcIPP GCN, BcPolyketide GCN, while G_h stands for Host genotypes. Interactions among the terms were not tested to avoid the potential for overfitting. AtNeti stands for one of the four Arabidopsis GCNs (e.g. AtDefense/Camalexin GCN, AtPlastid GCN, AtCell/Division GCN, AtPSI GCN). All multi-factor ANOVA models were optimized by trimming to just the terms with a significant *P*-value (*P*-value < 0.05).

Data Availability

The datasets in this study are available in the following database: Bioproject PRJNA473829 (https://www.ncbi.nlm.nih.gov/bioproject/?term=PRJNA473829). The computer scripts used in this study are available in GitHub (https://github.com/WeiZhang317/octopus).

Author contributions and Acknowledgement

JAC, DJK conceived and designed the experiments. JAC, WZ, DC, JF and RE performed the experiments. WZ, SA, DEC and DJK analyzed the data. WZ, JAC, and DJK wrote the paper.

Funding

Funding for this work was provided by the NSF award IOS 1339125 to DJK, the USDA National Institute of Food and Agriculture, Hatch project number CA-D-PLS-7033-H to DJK and by the Danish National Research Foundation (DNRF99) grant to DJK, the China Scholarship Council grant 20130624 to WZ.

Figure legends

Figure 1. Correlation between earlier estimated *B. cinerea* biomass and later lesion area. Model-corrected lesion area means were estimated using the linear model on the six replicates

data from three Arabidopsis genotypes at 72-hours post-infection with 96 *B. cinerea* isolates. Estimated biomass of *B. cinerea* was calculated using the linear model-corrected fraction of *B. cinerea* mapped reads against total mapped reads to Arabidopsis and *B. cinerea* reference genomes. RNA-Seq analysis was conducted at 16-hours post-infection for each pathosystem. Three Arabidopsis genotypes are wild-type Col-0 (purple dot), jasmonate insensitive mutant *coi1-1* (green triangle), and salicylic acid insensitive mutant *npr1-1* (orange diamond). The 90% confidence ellipse intervals are plotted for each Arabidopsis genotype for references. Quadratic regression lines are: Col-0: $y = -0.00059x^2 + 0.729x + 10.037$, $P = 0.0016$, adjusted $R^2 = 0.1101$; *coi1-1*: $y = -0.117x^2 + 4.44x - 0.1585$, $P = 3.914e-07$, adjusted $R^2 = 0.2562$; *npr1-1*: $y = -0.0579x^2 + 2.26x + 1.673$, $P = 0.0001$, adjusted $R^2 = 0.161$.

Figure 2. Transcriptomic responses of *B. cinerea* on Arabidopsis are controlled by genetic variation in pathogen population, host genotypes, and their interaction. (A) Distribution of broad-sense heritability (H^2) of *B. cinerea* transcripts contributed by genetic variation in the *B. cinerea*, Arabidopsis genotypes, and the interaction between pathogen and host. Violin plots illustrating the distribution of H^2 for transcripts from 96 *B. cinerea* isolates infecting on Arabidopsis genotypes. Heritability is partitioned across the different sources, 96 pathogen genotypes = "Isolate", plant genotypes Col-0, *coi1-1* and *npr1-1* plant genotypes = "Host", and the corresponding interaction. The transcriptomic analysis was conducted by sequencing mRNA extracted from *B. cinerea* infected Arabidopsis leaves at 16-hours post-infection. Red lines indicate the average broad-sense heritability values of lesion area caused by isolates, Arabidopsis genotypes, and their interaction. (B) to (E) Expression profiles of *B. cinerea* transcripts significantly influenced by host genotypes. The model-corrected means (log_2) for *B. cinerea* transcript were used for plotting. The Arabidopsis genotypes, wild-type Col-0 (purple), jasmonate insensitive mutant *coi1-1* (green), and salicylic acid mutant *npr1-1* (orange), are shown on the x axis. *B. cinerea* transcripts are: (B) *Bcin01g03790.1*, class IV chitin synthase; (C) *Bcin02g02980.1*, Monooxygenase; (D*) Bcin10g02260.1*, NADH oxidoreductase; (E) *Bcin11g05200.1*, caffeine-induced death Cid2; (F) to (I) Expression profiles of *B. cinerea* transcripts significantly influenced by the interaction between pathogen and host genotypes. (F) *Bcin02g03810.1*, GTP cyclohydrolase; (G) *Bcin09g01190.1*, Tripeptidyl-peptidase 1; (H) *Bcin10g01130.1*, in secretory pathway; (I) *Bcin14g05090.1*, a transcription factor.

Figure 3. Expression profiles of an endopolygalacturonase gene *Bcpg1* from diverse *B. cinerea* isolates across Arabidopsis genotypes. Rank plot shows the relationship of *Bcpg1* expression from 32 diverse *B. cinerea* isolates (right) across three Arabidopsis genotypes (x axis). Three Arabidopsis genotypes are wild-type Col-0 (purple dot), jasmonate insensitive mutant *coi1-1* (green triangle), and salicylic acid mutant *npr1-1* (orange diamond). The model-corrected means (log_2) for the transcript of *Bcpg1* (*Bcin14g00850.1*) encoding an endopolygalacturonase gene are utilized for plotting. The transcript expression levels from the same isolate across three Arabidopsis genotypes are connected with a colored line. The names of 32 isolates are represented with the same colored lines as induced *Bcpg1* expression levels. Black lines indicate the expression levels of *Bcpg1* are higher in *coi1-1* and *npr1-1* than in Col-0. Red lines indicate the higher expression levels of *Bcpg1* in *coi1-1* but lower in *npr1-1*. Blue lines indicate the highest expression levels of *Bcpg1* are in Col-0. Dark green lines indicate the higher expression levels of *Bcpg1* in *npr1-1* but lower in *coi1-1*.

Figure 4. Gene co-expression networks identified from *B. cinerea* transcriptomic responses to Arabidopsis wild-type Col-0 immunity. Ten gene co-expression networks (GCNs) with more than five nodes were identified from 96 *B. cinerea* isolates infecting on Arabidopsis wild-type Col-0. The similarity matrix is computed using Spearman's rank correlation coefficient. Nodes with different colors represent *B. cinerea* genes condensed in GCNs with different biological functions. Edges represent the Spearman's rank correlation coefficients between gene pairs. Trans- and cis-GCNs means GCNs are regulated by trans- and cis-regulatory elements, respectively. GCNs were named after their biological functions, which were determined by hub and bottleneck genes within each network. GCNs are: vesicle/virulence (red), translation/growth (green), exocytosis regulation (pink), cyclic peptide (yellow), peptidase (gray), isopentenyl pyrophosphate (IPP, turquoise), polyketide (violet), botcinic acid (BOA, blue), copper transport (slate blue), botrydial (BOT, purple).

Figure 5. Variation of transcripts accumulation for secondary metabolites production across diverse *B. cinerea* isolates. Expression profiles of genes responsible for botrydial, botcinic acid, cyclic peptide production across 96 isolates under Arabidopsis wild-type Col-0 are shown. **(**A) Schematic shows the genomic locus of seven botrydial (BOT) biosynthesis genes clustered together. Exons are represented by gray boxes. Introns and intergenic regions are represented by the grey line. Seven BOT genes are: *BcBOT1, BcBOT3* and *BcBOT4,* encoding a

724 cytochrome P450 monooxygenase, respectively; *BcBOT2* encoding a sesquiterpene cyclase;
725 *BcBOT5* encoding an acetyl transferase; *BcBOT6* encoding a Zn(II)2Cys6 transcription factor,
726 *BcBOT7* encoding a dehydrogenase reductase. (B) BOT biosynthesis pathway in *B. cinerea*. (C)
727 Bar plots compare expression variation of *BcBOT*2 across 96 *B. cinerea* isolates in responding to
728 Arabidopsis wild-type Col-0 immunity. The model-corrected means (log_2) of transcripts were
729 used for plotting. (D) Scatter plot illustrates the positive correlations between lesion area and
730 accumulation of *BcBOT2* transcript across the 96 isolates in response to varied Arabidopsis
731 immunities. Model-corrected lesion area means were estimated for three Arabidopsis genotypes
732 at 72-hours post-infection with 96 *B. cinerea* isolates. The three Arabidopsis genotypes are
733 labeled next to the confidence ellipse curves: wild-type Col-0 (purple dot), jasmonate insensitive
734 mutant *coi1-1* (green triangle), and salicylic acid mutant *npr1-1* (orange diamond). The 90%
735 confidence ellipse intervals are plotted for each Arabidopsis genotype for reference. Linear
736 regression lines: Col-0: y = 3.2532x + 4.4323, *P* = 1.008e-10, Adjusted R^2 = 3.3537; *coi1-1*: y =
737 7.4802x + 10.3289, *P* = 7.895e-15, adjusted R^2 = 0.4700; *npr1-1*: y = 3.7086x + 7.3487, *P* =
738 2.425e-11, adjusted R^2 = 0.3726. (E) and (F) Bar plots compare expression variation of *BcBOA6*
739 in botcinic acid (BOA) pathway and *Bcin01g11460.* in cyclic peptide pathway across 96 *B.*
740 *cinerea* isolates in response to Arabidopsis wild-type Col-0 immunity. (G) Venn diagram
741 illustrates the number of *B. cinerea* isolates with the ability to induce BOT, BOA, and cyclic
742 peptide.

743 **Figure 6. Comparison of plasticity of *B. cinerea* gene co-expression network under vaired**
744 **host immunity.** *B. cinerea* gene co-expression networks (GCNs) of vesicle/virulence (red) and
745 translation/growth (green) identified under three Arabidopsis genotypes are compared. Three
746 Arabidopsis genotypes are wild-type Col-0, jasmonate insensitive mutant *coi1-1*, and salicylic
747 acid mutant *npr1-1*. Nodes marked with red and green colors represent *B. cinerea* genes
748 condensed in GCNs with different biological functions. The same node condensed in GCNs
749 across three Arabidopsis genotypes was marked with same color. Nodes specificaly condensed in
750 GCNs under two mutants *coi1-1* and *npr1-1* background are marked with orange color. Edges
751 represent the Spearman's rank correlation coefficients between gene pairs.

752 **Figure 7. A dual interaction network reveals links between Arabidopsis immunity and *B.***
753 ***cinerea* virulence.** A dual interaction network was constructed using gene co-expression
754 networks (GCNs) from Arabidopsis and *B. cinerea* co-transcriptome. The first eigenvectors were

derived from individual GCNs and used as input to calculate Spearman's rank correlation coefficiency between GCN pairs. Green dots and orange triangles represent Arabidopsis immune- and *B. cinerea* virulence-GCNs, respectively. Blue and red lines (edges) represent the positive and negative Spearman's rank correlation coefficients between GCN pairs, respectively. The thickness of line signifies the correlational strength.

Supplemental Data

Supplemental Figure 1. **Expression profiles of an oxaloacetate hydrolase gene *Bcoah* from diverse *B. cinerea* isolates across Arabidopsis genotypes.** Rank plot shows the relationship o *Bcoah* expression from 32 diverse *B. cinerea* isolates (right) across three Arabidopsis genotypes (x axis). Three Arabidopsis genotypes are wild-type Col-0 (purple dot), jasmonate insensitive mutant *coi1-1* (green triangle), and salicylic acid mutant *npr1-1* (orange diamond). The model-corrected means (log_2) for the transcript of *Bcoah* (*Bcin12g01020.1*) encoding an oxaloacetate hydrolase gene are utilized for plotting. The transcript expression levels from the same isolate across three Arabidopsis genotypes are connected with a colored line. The names of 32 isolates are represented with the same colored lines as induced *Bcoah* expression levels. Black lines indicate the expression levels of *Bcoah* are higher in *coi1-1* and *npr1-1* than in Col-0. Red lines indicate the higher expression levels of *Bcoah* in *coi1-1* but lower in *npr1-1*. Blue lines indicate the highest expression levels of *Bcoah* are in Col-0. Dark green lines indicate the higher expression levels of *Bcoah* in *npr1-1* but lower in *coi1-1*.

Supplemental Figure 2. Gene co-expression networks identified from *B. cinerea* transcriptomic responses to Arabidopsis wild-type Col-0 immunity. *B. cinerea* gene co-expression networks (GCNs) were identified from 96 *B. cinerea* isolates infecting on Arabidopsis wild-type Col-0. The similarity matrix is computed using Spearman's rank correlation coefficient. All co-expressed gene pairs with correlation greater than 0.85 were shown. Nodes with different colors represent *B. cinerea* genes condensed in GCNs with different biological functions. Edges represent the Spearman's rank correlation coefficients between gene pairs. GCNs were ordered as number of nodes within each network. GCNs were named after their biological functions, which were determined by hub and bottleneck genes within each network: vesicle/virulence (red), translation/growth (green), botcinic acid (BOA, blue),

784 exocytosis regulation (pink), cyclic peptide (yellow), copper transport (slate blue), botrydial
785 (BOT, purple), peptidase (gray), isopentenyl pyrophosphate (IPP, turquoise), polyketide (violet).

786 **Supplemental Figure 3. Genomic location of *B. cinerea* gene co-expression networks.** The
787 circle diagrams showed the genome-wide distribution of gene pairs identified by *B. cinerea* gene
788 co-expression networks (GCNs) under Arabidopsis wild-type Col-0. (A) to (J) Genomic
789 locations of gene pairs identified by GCNs: (A) Vesicle/virulence, (B) translation/growth, (C)
790 botcinic acid (BOA), (D) exocytosis regulation, (E) cyclic peptide, (F) copper transport, (G)
791 botrydial (BOT), (H) peptidase (gray), (I) isopentenyl pyrophosphate (IPP), (G) polyketide. The
792 rings show 18 *B. cinerea* chromosomes on a Mb scale. Genomic locations of co-expressed gene
793 pairs are connected by the colored lines.

794 **Supplemental Figure 4. Gene co-expression networks identified from *B. cinerea***
795 **transcriptomic responses to Arabidopsis jasmonate-compromised immunity.** *B. cinerea*
796 gene co-expression networks (GCNs) were identified from 96 *B. cinerea* isolates infecting on
797 Arabidopsis jasmonate insensitive mutant *coi1-1*. The similarity matrix is computed using
798 Spearman's rank correlation coefficient. All co-expressed gene pairs with correlation greater
799 than 0.8 were shown. Nodes with different colors represent *B. cinerea* genes condensed in GCNs
800 with different biological functions. Nodes were marked with same color as under Arabidopsis
801 wild-type Col-0 background. Nodes specificaly condenced in GCNs under Arabidopsis mutant
802 *coi1-1* background are marked with orange color. Edges represent the Spearman's rank
803 correlation coefficients between gene pairs. GCNs were ordered as number of nodes within each
804 network. GCNs were named after their biological functions, which were determined by hub and
805 bottleneck genes within each network: vesicle/virulence (red/orange), translation/growth
806 (green/orange), botrydial/ isopentenyl pyrophosphate (BOT/IPP, blue/turquoise/orange), botcinic
807 acid (BOA, blue), exocytosis regulation (pink), peptidase (gray/orange), copper transport (slate
808 blue/orange), plant cell wall degradation (orange), cyclic peptide (yellow), peptidase II
809 (red/orange), siderophores (orange), 26S proteasome regulated protein degradation (red/orange),
810 sugar, ROS/NO stress (orange), ATP (orange), polyketide (violet/orange).

811 **Supplemental Figure 5. Gene co-expression networks identified from *B. cinerea***
812 **transcriptomic responses to Arabidopsis salicylic acid-compromised immunity.** *B. cinerea*
813 gene co-expression networks (GCNs) were identified from 96 *B. cinerea* isolates infecting on

814 Arabidopsis salicylic acid insensitive mutant *npr1-1*. The similarity matrix is computed using
815 Spearman's rank correlation coefficient. All co-expressed gene pairs with correlation greater
816 than 0.8 were shown. Nodes with different colors represent *B. cinerea* genes condensed in GCNs
817 with different biological functions. Nodes were marked with same color as under Arabidopsis
818 wild-type Col-0 background. Nodes specificaly condenced in GCNs under Arabidopsis mutant
819 *npr1-1* background are marked with orange color. Edges represent the Spearman's rank
820 correlation coefficients between gene pairs. GCNs were ordered as number of nodes within each
821 network. GCNs were named after their biological functions, which were determined by hub and
822 bottleneck genes within each network: translation/growth (green/orange), vesicle/virulence
823 (red/orange), peptidase (gray/orange), polyketide (violet/orange), botrydial/isopentenyl
824 pyrophosphate (BOT/IPP, blue/turquoise/orange), botcinic acid (BOA, blue), exocytosis
825 regulation (pink), copper transport (slate blue/orange), cyclic peptide (yellow), unknown (red),
826 sugar (orange), peptidase II (red/orange).

827 **Supplemental Figure 6. Plasticity in expression profiles of genes identified by *B. cinerea***
828 **gene co-expression networks under vairied Arabidopsis immunities.** Violin plots of (A) to
829 (O) show the expression profiles of *B. cinerea* genes in response to variation of Arabidopsis
830 immunity. Genes shown are condensed in *B. cinerea* gene co-expression networks (GCNs). The
831 model-corrected means ($\log_2$) for *B. cinerea* transcript were used for plotting. The Arabidopsis
832 genotypes, wild-type Col-0 (purple), jasmonate insensitive mutant *coi1-1* (green), and salicylic
833 acid mutant *npr1-1* (orange), are shown on the x axis.

834 **Supplemental Figure 7. Cross-kingdom Arabidopsis-*B. cinerea* gene co-expression**
835 **networks.** Three Arabidopsis genotypes are wild-type Col-0, jasmonate insensitive mutant *coi1-*
836 *1*, and salicylic acid insensitive mutant *npr1-1*. Green nodes represent Arabidopsis genes.
837 Orange, red and violet nodes represent *B. cinerea* genes. Nodes with red and violet colors are
838 condensed in *B. cinerea* vesicle/virulence and BOT gene co-expression networks, respectively.
839 The degree of a node is shown by the size of a node. Edges represent the Spearman's rank
840 correlation coefficients between gene pairs.

841 **Supplemental Figure 8. Associations between gene co-expression networks identified from**
842 **co- and single-transcriptome.** Venn diagrams highlights: (A) the overlap of plant (left) and
843 pathogen (right) genes condensed in Arabidopsis-*B. cinerea* gene co-expression networks

(GCNs) across three Arabidopsis genotypes, (B) the overlap of plant genes in Arabidopsis-B. cinerea GCNs and Arabidopsis GCNs across three genotypes, (C) the overlap of pathogen genes in Arabidopsis-*B. cinerea* GCNs and *B. cinerea* GCNs across three genotypes.

Supplemental Table 1. Topology traits of *B. cinerea in planta* gene co-expression networks.

Supplemental Table 2. ANOVA table of lesion area and *B. cinerea* pathways. A mixed linear model was fitted to test lesion area and *B. cinerea* pathways responsible for botrydial (BOT), botcinic acid (BOA), and cyclic peptide (CycPep) produced under three Arabidopsis genotypes. The lesion area data used in the model were GLM corrected least square means induced by 96 *B. cinerea* isolates. Model-corrected means of transcripts from 96 *B. cinerea* isolates were z-scaled and used in ANOVA. Df is the degrees of freedom for a term within the model. SS is the Sum of Squares variation. MS is the Mean of Squared variation. F value is derived from the F statistic and *P*-value indicates the statistical significance for a given term within the model. Significance of differences are shown as $P < 0.001$ '***', 0.01'**' and 0.05 '*'.

Supplemental Table 3. ANOVA tables of *B. cinerea* gene co-expression networks. Mixed linear models were fitted to individual *B. cinerea* (Bc) gene co-expression networks (GCNs) and variation of host genotypes and Arabidopsis (At) GCNs. Variation was estimated among host genotypes and first eigenvectors from four individual Arabidopsis GCNs. Df is the degrees of freedom for a term within the model. SS is the Sum of Squares variation. MS is the Mean of Squared variation. F value is derived from the F statistic and *P*-value indicates the statistical significance for a given term within the model. Significance of difference are shown as $P < 0.001$ '***', 0.01'**' and 0.05 '*'.

Supplemental Table 4. **ANOVA tables of Arabidopsis gene co-expression networks.** Linear mixed models were fitted to individual Arabidopsis (At) gene co-expression networks (GCNs) and variation of host genotypes and ten *B. cinerea* (Bc) GCNs. Variation was estimated among host genotypes and first eigenvectors from individual *B. cinerea* GCNs. Df is the degrees of freedom for a term within the model. SS is the Sum of Squares variation. MS is the Mean of Squared variation. F value is derived from the F statistic and *P*-value indicates the statistical significance for a given term within the model. Significance of difference are shown as $P < 0.001$ '***', 0.01'**' and 0.05 '*'.

Supplemental Table 5. Topology traits of cross-kingdom Arabidopsis-*B. cinerea* gene co-expression networks. Three Arabidopsis genotypes are wild-type Col-0, jasmonate insensitive mutant *coi1-1*, and salicylic acid insensitive mutant *npr1-1*.

Supplemental Data Set 1. Model-corrected means of *B. cinerea* transcripts. A table of model-corrected least-square means of *B. cinerea* transcripts from 96 isolates infection on Arabidopsis wild-type Col-0, jasmonate insensitive mutant *coi1-1*, and salicylic acid insensitive mutant *npr1-1*.

Supplemental Data Set 2. Standard errors of *B. cinerea* transcripts. A table of model-corrected standard errors of *B. cinerea* transcripts infection on Arabidopsis wild-type Col-0, jasmonate insensitive mutant *coi1-1*, and salicylic acid insensitive mutant *npr1-1*.

Supplemental Data Set 3. GLM deviance tables and broad-sense heritability of *B. cinerea* transcripts. Summary of deviance tables derived from generalized linear model and estimated broad-sense heritability (H^2) for *B. cinerea* transcripts. All significance values are corrected by false discovery rate.

Supplemental Data Set 4. Model-corrected means of estimated *B. cinerea* biomass. *B. cinerea* biomass of 96 isolates infection on Arabidopsis genotypes was estimated using the fraction of uniquely mapped reads against B05.10 reference genome. Three Arabidopsis genotypes are wild-type Col-0, jasmonate insensitive mutant *coi1-1*, and salicylic acid insensitive mutant *npr1-1*.

Supplemental Data Set 5. Top 100 heritability of *B. cinerea* transcripts. Broad-sense heritability (H^2) of individual *B. cinerea* transcript contributed by pathogen, host and their interaction were estimated. Three Arabidopsis genotypes are wild-type Col-0, jasmonate insensitive mutant *coi1-1*, and salicylic acid insensitive mutant *npr1-1*.

Supplemental Data Set 6. Spearman's rank correlation between lesion area and *B. cinerea* transcripts abundance. A table of spearman's rank correlation coefficiency between lesion area and *B. cinerea* transcripts accumulation across three Arabidopsis genotypes or under individual genotypes. Three Arabidopsis genotypes are wild-type Col-0, jasmonate insensitive mutant *coi1-1*, and salicylic acid insensitive mutant *npr1-1*.

Supplemental Data Set 7. Gene list of *B. cinerea* gene co-expression networks. Tables of *B. cinerea* genes identified by *B. cinerea* gene co-expression networks (GCNs) during 96 isolates infection on Arabidopsis wild-type Col-0, jasmonate insensitive mutant *coi1-1*, and salicylic acid insensitive mutant *npr1-1*.

Supplemental Data Set 8. Gene list of cross-kingdom Arabidopsis-*B. cinerea* gene co-expression networks. Tables of Arabidopsis and *B. cinerea* genes identified by co-transcriptome gene co-expression networks (GCNs) during 96 isolates infection on Arabidopsis wild-type Col-0, jasmonate insensitive mutant *coi1-1*, and salicylic acid insensitive mutant *npr1-1*.

References

Arbelet, D., Malfatti, P., Simond-Cote, E., Fontaine, T., Desquilbet, L., Expert, D., Kunz, C., and Soulie, M.C. (2010). Disruption of the Bcchs3a chitin synthase gene in Botrytis cinerea is responsible for altered adhesion and overstimulation of host plant immunity. Mol. Plant Microbe Interact. **23,** 1324-1334, doi/10.1094/MPMI-02-10-0046.

Ascari, J., Boaventura, M.A., Takahashi, J.A., Duran-Patron, R., Hernandez-Galan, R., Macias-Sanchez, A.J., and Collado, I.G. (2013). Phytotoxic activity and metabolism of Botrytis cinerea and structure-activity relationships of isocaryolane derivatives. J. Nat. Prod. **76,** 1016-1024, doi/10.1021/np3009013.

Atwell, S., Corwin, J.A., Soltis, N.E., Subedy, A., Denby, K.J., and Kliebenstein, D.J. (2015). Whole genome resequencing of Botrytis cinerea isolates identifies high levels of standing diversity. Front. Microbiol. **6,** 996, doi/10.3389/fmicb.2015.00996.

Bednarek, P., Pislewska-Bednarek, M., Svatos, A., Schneider, B., Doubsky, J., Mansurova, M., Humphry, M., Consonni, C., Panstruga, R., Sanchez-Vallet, A., Molina, A., and Schulze-Lefert, P. (2009). A glucosinolate metabolism pathway in living plant cells mediates broad-spectrum antifungal defense. Science **323,** 101-106, doi/10.1126/science.1163732.

Benjamini Yoav and Yekutieli Daniel (2001). The Control of the False Discovery Rate in Multiple Testing under Dependency. **29,** 1165-1188, doi/10.1214/aos/1013699998.

Benton, M.J. (2009). The Red Queen and the Court Jester: species diversity and the role of biotic and abiotic factors through time. Science **323,** 728-732, doi/10.1126/science.1157719.

Bergelson, J., Kreitman, M., Stahl, E.A., and Tian, D. (2001). Evolutionary dynamics of plant R-genes. Science **292,** 2281-2285, doi/10.1126/science.1061337.

Blanco-Ulate, B., Morales-Cruz, A., Amrine, K.C., Labavitch, J.M., Powell, A.L., and Cantu, D. (2014). Genome-wide transcriptional profiling of Botrytis cinerea genes targeting plant cell walls during infections of different hosts. Front. Plant. Sci. **5,** 435, doi/10.3389/fpls.2014.00435.

Brooks, D.M., Bender, C.L., and Kunkel, B.N. (2005). The Pseudomonas syringae phytotoxin coronatine promotes virulence by overcoming salicylic acid-dependent defences in Arabidopsis thaliana. Mol. Plant. Pathol. **6,** 629-639, doi/10.1111/j.1364-3703.2005.00311.x.

Bullard, J.H., Purdom, E., Hansen, K.D., and Dudoit, S. (2010). Evaluation of statistical methods for normalization and differential expression in mRNA-Seq experiments. BMC Bioinformatics **11,** 94, doi/10.1186/1471-2105-11-94.

Buttner, D. and He, S.Y. (2009). Type III protein secretion in plant pathogenic bacteria. Plant Physiol. **150,** 1656-1664, doi/10.1104/pp.109.139089.

Cantarel, B.L., Coutinho, P.M., Rancurel, C., Bernard, T., Lombard, V., and Henrissat, B. (2009). The Carbohydrate-Active EnZymes database (CAZy): an expert resource for Glycogenomics. **37,** D233–D238, doi/10.1093/nar/gkn663.

Cao, H., Glazebrook, J., Clarke, J.D., Volko, S., and Dong, X. (1997). The Arabidopsis NPR1 gene that controls systemic acquired resistance encodes a novel protein containing ankyrin repeats. Cell **88,** 57-63, doi/10.1016/S0092-8674(00)81858-9.

Choquer, M., Fournier, E., Kunz, C., Levis, C., Pradier, J.M., Simon, A., and Viaud, M. (2007). Botrytis cinerea virulence factors: new insights into a necrotrophic and polyphageous pathogen. FEMS Microbiol. Lett. **277,** 1-10, doi/10.1111/j.1574-6968.2007.00930.x.

Clay, N.K., Adio, A.M., Denoux, C., Jander, G., and Ausubel, F.M. (2009). Glucosinolate metabolites required for an Arabidopsis innate immune response. Science **323,** 95-101, doi/10.1126/science.1164627.

Colmenares, A.J., Aleu, J., Duran-Patron, R., Collado, I.G., and Hernandez-Galan, R. (2002). The putative role of botrydial and related metabolites in the infection mechanism of Botrytis cinerea. J. Chem. Ecol. **28,** 997-1005, doi/1015209817830.

Colombo, M., Raposo, G., and Thery, C. (2014). Biogenesis, secretion, and intercellular interactions of exosomes and other extracellular vesicles. Annu. Rev. Cell Dev. Biol. **30,** 255-289, doi/10.1146/annurev-cellbio-101512-122326.

Conesa, A., Gotz, S., Garcia-Gomez, J.M., Terol, J., Talon, M., and Robles, M. (2005). Blast2GO: a universal tool for annotation, visualization and analysis in functional genomics research. Bioinformatics **21,** 3674-3676, doi/10.1093/bioinformatics/bti610.

Corwin, J.A., Copeland, D., Feusier, J., Subedy, A., Eshbaugh, R., Palmer, C., Maloof, J., and Kliebenstein, D.J. (2016). The Quantitative Basis of the Arabidopsis Innate Immune System to Endemic Pathogens Depends on Pathogen Genetics. PLoS Genet. **12,** e1005789, doi/10.1371/journal.pgen.1005789.

Corwin, J.A., Subedy, A., Eshbaugh, R., and Kliebenstein, D.J. (2016). Expansive Phenotypic Landscape of Botrytis cinerea Shows Differential Contribution of Genetic Diversity and Plasticity. Mol. Plant Microbe Interact. **29,** 287-298, doi/10.1094/MPMI-09-15-0196-R.

Corwin, J.A. and Kliebenstein, D.J. (2017). Quantitative Resistance: More Than Just Perception of a Pathogen. Plant Cell **29,** 655-665, doi/10.1105/tpc.16.00915.

Courtade, G., Wimmer, R., Røhr, ÅK., Preims, M., Felice, A.K.G., Dimarogona, M., Vaaje-Kolstad, G., Sørlie, M., Sandgren, M., Ludwig, R., Eijsink, V.G.H., and Aachmann, F.L. (2016). Interactions of a fungal lytic polysaccharide monooxygenase with β-glucan substrates and cellobiose dehydrogenase. **113,** 5922, doi/10.1073/pnas.1602566113.

Couto, D. and Zipfel, C. (2016). Regulation of pattern recognition receptor signalling in plants. Nat. Rev. Immunol. **16,** 537-552, doi/10.1038/nri.2016.77.

Cui, H., Qiu, J., Zhou, Y., Bhandari, D.D., Zhao, C., Bautor, J., and Parker, J.E. (2018). Antagonism of Transcription Factor MYC2 by EDS1/PAD4 Complexes Bolsters Salicylic Acid Defense in Arabidopsis Effector-Triggered Immunity. Mol. Plant. **11,** 1053-1066, doi/10.1016/j.molp.2018.05.007.

Dalmais, B., Schumacher, J., Moraga, J., LE Pêcheur, P., Tudzynski, B., Collado, I.G., and Viaud, M. (2011). The Botrytis cinerea phytotoxin botcinic acid requires two polyketide synthases for production and has a redundant role in virulence with botrydial. **12,** 564, doi/10.1111/j.1364-3703.2010.00692.x.

Dangl, J.L. and Jones, J.D. (2001). Plant pathogens and integrated defence responses to infection. Nature **411,** 826-833, doi/10.1038/35081161.

Deighton, N., Muckenschnabel, I., Colmenares, A.J., Collado, I.G., and Williamson, B. (2001). Botrydial is produced in plant tissues infected by Botrytis cinerea. Phytochemistry **57,** 689-692, doi/10.1016/S0031-9422(01)00088-7.

Denby, K.J., Kumar, P., and Kliebenstein, D.J. (2004). Identification of Botrytis cinerea susceptibility loci in Arabidopsis thaliana. Plant J. **38,** 473-486, doi/10.1111/j.0960-7412.2004.02059.x.

Ding Qiong and Zhang Jinlong (2012). seqRFLP: Simulation and visualization of restriction enzyme cutting pattern from DNA sequences. **R package version 1.0.1.,** .

Fordyce, R.F., Soltis, N.E., Caseys, C., Gwinner, R., Corwin, J.A., Atwell, S., Copeland, D., Feusier, J., Subedy, A., Eshbaugh, R., and Kliebenstein, D.J. (2018). Digital Imaging Combined with Genome-Wide Association Mapping Links Loci to Plant-Pathogen Interaction Traits. Plant Physiol., doi/10.1104/pp.18.00851.

Fox, J. and Weisberg, S. (2011). An R Companion to Applied Regression, Second Edition ed. (Sage, CA: Thousand Oaks).

Frerigmann, H., Pislewska-Bednarek, M., Sanchez-Vallet, A., Molina, A., Glawischnig, E., Gigolashvili, T., and Bednarek, P. (2016). Regulation of Pathogen-Triggered Tryptophan Metabolism in Arabidopsis thaliana by MYB Transcription Factors and Indole Glucosinolate Conversion Products. Mol. Plant. **9,** 682-695, doi/10.1016/j.molp.2016.01.006.

Gerbi, C., Bata, J., Breton, A., and Prensier, G. (1996). Glycoside and polysaccharide hydrolase activity of the rumen anaerobic fungus Caecomyces communis (Sphaeromonas communis SENSU ORPIN) at early and final stages of the developmental cycle. Curr. Microbiol. **32,** 256-259, doi/10.1007/s002849900046.

Glazebrook, J. (2005). Contrasting mechanisms of defense against biotrophic and necrotrophic pathogens. Annu. Rev. Phytopathol. **43,** 205-227, doi/10.1146/annurev.phyto.43.040204.135923.

Gotz, S., Garcia-Gomez, J.M., Terol, J., Williams, T.D., Nagaraj, S.H., Nueda, M.J., Robles, M., Talon, M., Dopazo, J., and Conesa, A. (2008). High-throughput functional annotation and data mining with the Blast2GO suite. Nucleic Acids Res. **36,** 3420-3435, doi/10.1093/nar/gkn176.

Govrin, E.M. and Levine, A. (2000). The hypersensitive response facilitates plant infection by the necrotrophic pathogen Botrytis cinerea. Curr. Biol. **10,** 751-757, doi/10.1016/S0960-9822(00)00560-1.

Greenberg, J.T., Guo, A., Klessig, D.F., and Ausubel, F.M. (1994). Programmed cell death in plants: a pathogen-triggered response activated coordinately with multiple defense functions. Cell **77,** 551-563, doi/10.1016/0092-8674(94)90217-8.

Igarashi, K., Uchihashi, T., Uchiyama, T., Sugimoto, H., Wada, M., Suzuki, K., Sakuda, S., Ando, T., Watanabe, T., and Samejima, M. (2014). Two-way traffic of glycoside hydrolase family 18 processive chitinases on crystalline chitin. Nat. Commun. **5,** 3975, doi/10.1038/ncomms4975.

Ingo Morgenstern, Justin Powlowski, and Adrian Tsang (2014). Fungal cellulose degradation by oxidative enzymes: from dysfunctional GH61 family to powerful lytic polysaccharide monooxygenase family. **13,** 471, doi/10.1093/bfgp/elu032.

Jones, J.D. and Dangl, J.L. (2006). The plant immune system. Nature **444,** 323-329, doi/10.1038/nature05286.

Kanzaki, H., Yoshida, K., Saitoh, H., Fujisaki, K., Hirabuchi, A., Alaux, L., Fournier, E., Tharreau, D., and Terauchi, R. (2012). Arms race co-evolution of Magnaporthe oryzae AVR-Pik and rice Pik genes driven by their physical interactions. Plant J. **72,** 894-907, doi/10.1111/j.1365-313X.2012.05110.x.

Karasov, T.L., Kniskern, J.M., Gao, L., DeYoung, B.J., Ding, J., Dubiella, U., Lastra, R.O., Nallu, S., Roux, F., Innes, R.W., Barrett, L.G., Hudson, R.R., and Bergelson, J. (2014). The long-term maintenance of a resistance polymorphism through diffuse interactions. Nature **512,** 436-440, doi/10.1038/nature13439.

Kliebenstein, D.J., Rowe, H.C., and Denby, K.J. (2005). Secondary metabolites influence Arabidopsis/Botrytis interactions: variation in host production and pathogen sensitivity. Plant J. **44,** 25-36, doi/10.1111/j.1365-313X.2005.02508.x.

Krishnakumar, V., Hanlon, M.R., Contrino, S., Ferlanti, E.S., Karamycheva, S., Kim, M., Rosen, B.D., Cheng, C.Y., Moreira, W., Mock, S.A., Stubbs, J., Sullivan, J.M., Krampis, K., Miller, J.R., Micklem, G., Vaughn, M., and Town, C.D. (2015). Araport: the Arabidopsis information portal. Nucleic Acids Res. **43,** 1003, doi/10.1093/nar/gku1200.

Kubicek, C.P., Starr, T.L., and Glass, N.L. (2014). Plant cell wall-degrading enzymes and their secretion in plant-pathogenic fungi. Annu. Rev. Phytopathol. **52,** 427-451, doi/10.1146/annurev-phyto-102313-045831.

Kumar, R., Ichihashi, Y., Kimura, S., Chitwood, D.H., Headland, L.R., Peng, J., Maloof, J.N., and Sinha, N.R. (2012). A High-Throughput Method for Illumina RNA-Seq Library Preparation. Front. Plant. Sci. **3,** 202, doi/10.3389/fpls.2012.00202.

Lamesch, P., Dreher, K., Swarbreck, D., Sasidharan, R., Reiser, L., and Huala, E. (2010). Using the Arabidopsis information resource (TAIR) to find information about Arabidopsis genes. Curr. Protoc. Bioinformatics **Chapter 1,** Unit1.11, doi/10.1002/cpbi.36.

Lamesch, P., Berardini, T.Z., Li, D., Swarbreck, D., Wilks, C., Sasidharan, R., Muller, R., Dreher, K., Alexander, D.L., Garcia-Hernandez, M., Karthikeyan, A.S., Lee, C.H., Nelson, W.D., Ploetz, L., Singh, S., Wensel, A., and Huala, E. (2012). The Arabidopsis Information Resource (TAIR): improved gene annotation and new tools. Nucleic Acids Res. **40,** 1202, doi/10.1093/nar/gkr1090.

Langfelder, P. and Horvath, S. (2008). WGCNA: an R package for weighted correlation network analysis. BMC Bioinformatics **9,** 559, doi/10.1186/1471-2105-9-559.

Langmead, B., Trapnell, C., Pop, M., and Salzberg, S.L. (2009). Ultrafast and memory-efficient alignment of short DNA sequences to the human genome. Genome Biol. **10,** r25. Epub 2009 Mar 4, doi/10.1186/gb-2009-10-3-r25.

Lanver, D., Muller, A.N., Happel, P., Schweizer, G., Haas, F.B., Franitza, M., Pellegrin, C., Reissmann, S., Altmuller, J., Rensing, S.A., and Kahmann, R. (2018). The Biotrophic Development of Ustilago maydis Studied by RNA-Seq Analysis. Plant Cell **30,** 300-323, doi/10.1105/tpc.17.00764.

Lee, H.J., Georgiadou, A., Walther, M., Nwakanma, D., Stewart, L.B., Levin, M., Otto, T.D., Conway, D.J., Coin, L.J., and Cunnington, A.J. (2018). Integrated pathogen load and dual transcriptome analysis of systemic host-pathogen interactions in severe malaria. Sci. Transl. Med. **10,** 10.1126/scitranslmed.aar3619, doi/10.1126/scitranslmed.aar3619.

Li, H., Handsaker, B., Wysoker, A., Fennell, T., Ruan, J., Homer, N., Marth, G., Abecasis, G., Durbin, R., and 1000 Genome Project Data Processing Subgroup (2009). The Sequence Alignment/Map format and SAMtools. Bioinformatics **25,** 2078-2079, doi/10.1093/bioinformatics/btp352.

Macheleidt, J., Mattern, D.J., Fischer, J., Netzker, T., Weber, J., Schroeckh, V., Valiante, V., and Brakhage, A.A. (2016). Regulation and Role of Fungal Secondary Metabolites. Annu. Rev. Genet. **50,** 371-392, doi/10.1146/annurev-genet-120215-035203.

McClure, R.S., Overall, C.C., Hill, E.A., Song, H.S., Charania, M., Bernstein, H.C., McDermott, J.E., and Beliaev, A.S. (2018). Species-specific transcriptomic network inference of interspecies interactions. ISME J. **12,** 2011-2023, doi/10.1038/s41396-018-0145-6.

Mengiste, T., Chen, X., Salmeron, J., and Dietrich, R. (2003). The BOTRYTIS SUSCEPTIBLE1 gene encodes an R2R3MYB transcription factor protein that is required for biotic and abiotic stress responses in Arabidopsis. Plant Cell **15,** 2551-2565, doi/10.1105/tpc.014167.

Mengiste, T. (2012). Plant immunity to necrotrophs. Annu. Rev. Phytopathol. **50,** 267-294, doi/10.1146/annurev-phyto-081211-172955.

Mine, A., Seyfferth, C., Kracher, B., Berens, M.L., Becker, D., and Tsuda, K. (2018). The Defense Phytohormone Signaling Network Enables Rapid, High-Amplitude Transcriptional Reprogramming during Effector-Triggered Immunity. Plant Cell **30,** 1199-1219, doi/10.1105/tpc.17.00970.

Mittal, S. and Davis, K.R. (1995). Role of the phytotoxin coronatine in the infection of Arabidopsis thaliana by Pseudomonas syringae pv. tomato. Mol. Plant Microbe Interact. **8,** 165-171.

Moraga, J., Dalmais, B., Izquierdo-Bueno, I., Aleu, J., Hanson, J.R., Hernandez-Galan, R., Viaud, M., and Collado, I.G. (2016). Genetic and Molecular Basis of Botrydial Biosynthesis: Connecting Cytochrome P450-Encoding Genes to Biosynthetic Intermediates. ACS Chem. Biol. **11,** 2838-2846, doi/10.1021/acschembio.6b00581.

Movahedi, S., Norey, C.G., Kay, J., and Heale, J.B. (1991). Infection and pathogenesis of cash crops by Botrytis cinerea: primary role of an aspartic proteinase. **306,** 213.

Musungu, B.M., Bhatnagar, D., Brown, R.L., Payne, G.A., OBrian, G., Fakhoury, A.M., and Geisler, M. (2016). A Network Approach of Gene Co-expression in the Zea mays/Aspergillus flavus Pathosystem to Map Host/Pathogen Interaction Pathways. Front. Genet. **7,** 206, doi/10.3389/fgene.2016.00206.

Nelson, C.E., Attia, M.A., Rogowski, A., Morland, C., Brumer, H., and Gardner, J.G. (2017). Comprehensive functional characterization of the glycoside hydrolase family 3 enzymes from Cellvibrio japonicus reveals unique metabolic roles in biomass saccharification. Environ. Microbiol. **19,** 5025-5039, doi/10.1111/1462-2920.13959.

Nobori, T., Velasquez, A.C., Wu, J., Kvitko, B.H., Kremer, J.M., Wang, Y., He, S.Y., and Tsuda, K. (2018). Transcriptome landscape of a bacterial pathogen under plant immunity. Proc. Natl. Acad. Sci. U. S. A. **115,** E3064, doi/10.1073/pnas.1800529115.

Okada, H., Ebhardt, H.A., Vonesch, S.C., Aebersold, R., and Hafen, E. (2016). Proteome-wide association studies identify biochemical modules associated with a wing-size phenotype in Drosophila melanogaster. Nat. Commun. **7,** 12649, doi/10.1038/ncomms12649.

Pages, H., Aboyoun, P., Gentleman, R., and DebRoy, S. (2017). Biostrings: String objects representing biological sequences, and matching algorithms. **R package version 2.44.2.,** .

Pérez-Izquierdo, L., Morin, E., Maurice, J.P., Martin, F., Rincón, A., and Buée, M. (2017). A new promising phylogenetic marker to study the diversity of fungal communities: The Glycoside Hydrolase 63 gene. **17,** e11, doi/10.1111/1755-0998.12678.

Pieterse, C.M. and Van Loon, L.C. (2004). NPR1: the spider in the web of induced resistance signaling pathways. Curr. Opin. Plant Biol. **7,** 456-464, doi/10.1016/j.pbi.2004.05.006.

Pinedo, C., Wang, C., Pradier, J., Dalmais, B., Choquer, M., Le Pêcheur, P., Morgant, G., Collado, I.G., Cane, D.E., and Viaud, M. (2008). Sesquiterpene synthase from the botrydial biosynthetic gene cluster of the phytopathogen Botrytis cinerea. **3,** 791, doi/10.1021/cb800225v.

Porquier, A., Morgant, G., Moraga, J., Dalmais, B., Luyten, I., Simon, A., Pradier, J.M., Amselem, J., Collado, I.G., and Viaud, M. (2016). The botrydial biosynthetic gene cluster of Botrytis cinerea displays a bipartite genomic structure and is positively regulated by the putative Zn(II)2Cys6 transcription factor BcBot6. Fungal Genet. Biol. **96,** 33-46, doi/10.1016/j.fgb.2016.10.003.

Poussereau, N., Creton, S., Billon-Grand, G., Rascle, C., and Fevre, M. (2001). Regulation of acp1, encoding a non-aspartyl acid protease expressed during pathogenesis of Sclerotinia sclerotiorum. Microbiology **147,** 717-726, doi/10.1099/00221287-147-3-717.

R Core Team (2014). R: A Language and Environment for Statistical Computing. (Vienna, Austria).

Robinson, M.D. and Smyth, G.K. (2008). Small-sample estimation of negative binomial dispersion, with applications to SAGE data. Biostatistics **9,** 321-332, doi/10.1093/biostatistics/kxm030.

Robinson, M.D. and Oshlack, A. (2010). A scaling normalization method for differential expression analysis of RNA-seq data. Genome Biol. **11,** r25. Epub 2010 Mar 2, doi/10.1186/gb-2010-11-3-r25.

Rodrigues, M.L., Godinho, R.M., Zamith-Miranda, D., and Nimrichter, L. (2015). Traveling into Outer Space: Unanswered Questions about Fungal Extracellular Vesicles. PLoS Pathog. **11,** e1005240, doi/10.1371/journal.ppat.1005240.

Rossi, F.R., Garriz, A., Marina, M., Romero, F.M., Gonzalez, M.E., Collado, I.G., and Pieckenstain, F.L. (2011). The sesquiterpene botrydial produced by Botrytis cinerea induces the hypersensitive response on plant tissues and its action is modulated by salicylic acid and jasmonic acid signaling. Mol. Plant Microbe Interact. **24,** 888-896, doi/10.1094/MPMI-10-10-0248.

Rowe, H.C. and Kliebenstein, D.J. (2007). Elevated genetic variation within virulence-associated Botrytis cinerea polygalacturonase loci. Mol. Plant Microbe Interact. **20,** 1126-1137, doi/10.1094/MPMI-20-9-1126.

Russell V. Lenth (2016). Least-Squares Means: The R Package lsmeans. **69,** 1-33, doi/10.18637/jss.v069.i01.

Samuel, M., Bleackley, M., Anderson, M., and Mathivanan, S. (2015). Extracellular vesicles including exosomes in cross kingdom regulation: a viewpoint from plant-fungal interactions. Front. Plant. Sci. **6,** 766, doi/10.3389/fpls.2015.00766.

Schumacher, J., Pradier, J.M., Simon, A., Traeger, S., Moraga, J., Collado, I.G., Viaud, M., and Tudzynski, B. (2012). Natural variation in the VELVET gene bcvel1 affects virulence and light-dependent differentiation in Botrytis cinerea. PLoS One **7,** e47840, doi/10.1371/journal.pone.0047840.

Schumacher, J., Simon, A., Cohrs, K.C., Traeger, S., Porquier, A., Dalmais, B., Viaud, M., and Tudzynski, B. (2015). The VELVET Complex in the Gray Mold Fungus Botrytis cinerea: Impact of BcLAE1 on Differentiation, Secondary Metabolism, and Virulence. Mol. Plant Microbe Interact. **28,** 659-674, doi/10.1094/MPMI-12-14-0411-R.

Shannon, P., Markiel, A., Ozier, O., Baliga, N.S., Wang, J.T., Ramage, D., Amin, N., Schwikowski, B., and Ideker, T. (2003). Cytoscape: a software environment for integrated models of biomolecular interaction networks. Genome Res. **13,** 2498-2504, doi/10.1101/gr.1239303.

Sharma, H.C., Pampapathy, G., Dhillon, M.K., and Ridsdill-Smith, J.T. (2005). Detached leaf assay to screen for host plant resistance to Helicoverpa armigera. J. Econ. Entomol. **98,** 568-576, doi/10.1603/0022-0493-98.2.568.

Siewers, V., Viaud, M., Jimenez-Teja, D., Collado, I.G., Gronover, C.S., Pradier, J., Tudzynski, B., and Tudzynski, P. (2005). Functional analysis of the cytochrome P450 monooxygenase gene bcbot1 of Botrytis cinerea indicates that botrydial is a strain-specific virulence factor. **18,** 602, doi/10.1094/MPMI-18-0602.

Soltis, N.E., Atwell, S., Shi, G., Fordyce, R., Gwinner, R., Gao, D., Shafi, A., and Kliebenstein, D. (2018). Crop domestication and pathogen virulence: Interactions of tomato and *Botrytis* genetic diversity. , doi/10.1101/255992.

Stefanato, F.L., Abou-Mansour, E., Buchala, A., Kretschmer, M., Mosbach, A., Hahn, M., Bochet, C.G., Metraux, J.P., and Schoonbeek, H.J. (2009). The ABC transporter BcatrB from Botrytis cinerea exports camalexin and is a virulence factor on Arabidopsis thaliana. Plant J. **58,** 499-510, doi/10.1111/j.1365-313X.2009.03794.x.

Stergiopoulos, I. and de Wit, P.J. (2009). Fungal effector proteins. Annu. Rev. Phytopathol. **47,** 233-263, doi/10.1146/annurev.phyto.112408.132637.

Stuart, J.M., Segal, E., Koller, D., and Kim, S.K. (2003). A gene-coexpression network for global discovery of conserved genetic modules. Science **302,** 249-255, doi/10.1126/science.1087447.

Swierzy, I.J., Handel, U., Kaever, A., Jarek, M., Scharfe, M., Schluter, D., and Luder, C.G.K. (2017). Divergent co-transcriptomes of different host cells infected with Toxoplasma gondii reveal cell type-specific host-parasite interactions. Sci. Rep. **7,** w, doi/10.1038/s41598-017-07838-w.

Tang, D., Wang, G., and Zhou, J.M. (2017). Receptor Kinases in Plant-Pathogen Interactions: More Than Pattern Recognition. Plant Cell **29,** 618-637, doi/10.1105/tpc.16.00891.

Tayal, P., Raj, S., Sharma, E., Kumar, M., Dayaman, V., Verma, N., Jogawat, A., Dua, M., Kapoor, R., and Johri, A.K. (2017). A Botrytis cinerea KLP-7 Kinesin acts as a Virulence Determinant during Plant Infection. Sci. Rep. **7,** 5, doi/10.1038/s41598-017-09409-5.

ten Have, A., Dekkers, E., Kay, J., Phylip, L.H., and van Kan, J.A. (2004). An aspartic proteinase gene family in the filamentous fungus Botrytis cinerea contains members with novel features. Microbiology **150,** 2475-2489, doi/10.1099/mic.0.27058-0.

ten Have, A., Espino, J.J., Dekkers, E., Van Sluyter, S.C., Brito, N., Kay, J., Gonzalez, C., and van Kan, J.A. (2010). The Botrytis cinerea aspartic proteinase family. Fungal Genet. Biol. **47,** 53-65, doi/10.1016/j.fgb.2009.10.008.

Tien-chye Tan, Daniel Kracher, Rosaria Gandini, Christoph Sygmund, Roman Kittl, Dietmar Haltrich, B Martin Hällberg, Roland Ludwig, and Christina Divne (2015). Structural basis for cellobiose dehydrogenase action during oxidative cellulose degradation. **6,** 7542, doi/10.1038/ncomms8542.

Toruno, T.Y., Stergiopoulos, I., and Coaker, G. (2016). Plant-Pathogen Effectors: Cellular Probes Interfering with Plant Defenses in Spatial and Temporal Manners. Annu. Rev. Phytopathol. **54,** 419-441, doi/10.1146/annurev-phyto-080615-100204.

Tsuda, K. and Katagiri, F. (2010). Comparing signaling mechanisms engaged in pattern-triggered and effector-triggered immunity. Curr. Opin. Plant Biol. **13,** 459-465, doi/10.1016/j.pbi.2010.04.006.

Urlacher, V.B. and Girhard, M. (2012). Cytochrome P450 monooxygenases: an update on perspectives for synthetic application. Trends Biotechnol. **30,** 26-36, doi/10.1016/j.tibtech.2011.06.012.

Van Kan, J.A., Stassen, J.H., Mosbach, A., Van Der Lee, T A, Faino, L., Farmer, A.D., Papasotiriou, D.G., Zhou, S., Seidl, M.F., Cottam, E., Edel, D., Hahn, M., Schwartz, D.C., Dietrich, R.A., Widdison, S., and Scalliet, G. (2017). A gapless genome sequence of the fungus Botrytis cinerea. Mol. Plant. Pathol. **18,** 75-89, doi/10.1111/mpp.12384.

Van Vu, B., Itoh, K., Nguyen, Q.B., Tosa, Y., and Nakayashiki, H. (2012). Cellulases belonging to glycoside hydrolase families 6 and 7 contribute to the virulence of Magnaporthe oryzae. Mol. Plant Microbe Interact. **25,** 1135-1141, doi/10.1094/MPMI-02-12-0043-R.

Venables, W.N. and Ripley, B.D. (2002). Modern Applied Statistics with S, Fourth Edition ed. (New York: Springer).

Walker, A.S., Gladieux, P., Decognet, V., Fermaud, M., Confais, J., Roudet, J., Bardin, M., Bout, A., Nicot, P.C., Poncet, C., and Fournier, E. (2015). Population structure and temporal maintenance of the multihost fungal pathogen Botrytis cinerea: causes and implications for disease management. Environ. Microbiol. **17,** 1261-1274, doi/10.1111/1462-2920.12563.

Walz, A., Zingen-Sell, I., Loeffler, M., and Sauer, M. (2008). Expression of an oxalate oxidase gene in tomato and severity of disease caused by Botrytis cinerea and Sclerotinia sclerotiorum. **57,** 453-458, doi/10.1111/j.1365-3059.2007.01815.x.

Wang, C.M., Hopson, R., Lin, X., and Cane, D.E. (2009). Biosynthesis of the sesquiterpene botrydial in Botrytis cinerea. Mechanism and stereochemistry of the enzymatic formation of presilphiperfolan-8beta-ol. J. Am. Chem. Soc. **131,** 8360-8361, doi/10.1021/ja9021649.

Weiberg, A., Wang, M., Lin, F.M., Zhao, H., Zhang, Z., Kaloshian, I., Huang, H.D., and Jin, H. (2013). Fungal small RNAs suppress plant immunity by hijacking host RNA interference pathways. Science **342,** 118-123, doi/10.1126/science.1239705.

Westermann, A.J., Barquist, L., and Vogel, J. (2017). Resolving host-pathogen interactions by dual RNA-seq. PLoS Pathog. **13,** e1006033, doi/10.1371/journal.ppat.1006033.

Williamson, B., Tudzynski, B., Tudzynski, P., and van Kan, J.A. (2007). Botrytis cinerea: the cause of grey mould disease. Mol. Plant. Pathol. **8,** 561-580, doi/10.1111/j.1364-3703.2007.00417.x.

Windram, O., Madhou, P., McHattie, S., Hill, C., Hickman, R., Cooke, E., Jenkins, D.J., Penfold, C.A., Baxter, L., Breeze, E., Kiddle, S.J., Rhodes, J., Atwell, S., Kliebenstein, D.J., Kim, Y.S., Stegle, O., Borgwardt, K., Zhang, C., Tabrett, A., Legaie, R., Moore, J., Finkenstadt, B., Wild, D.L., Mead, A., Rand, D., Beynon, J., Ott, S., Buchanan-Wollaston, V., and Denby, K.J. (2012). Arabidopsis defense against Botrytis cinerea: chronology and regulation deciphered by high-resolution temporal transcriptomic analysis. Plant Cell **24,** 3530-3557, doi/10.1105/tpc.112.102046.

Xie, D.X., Feys, B.F., James, S., Nieto-Rostro, M., and Turner, J.G. (1998). COI1: an Arabidopsis gene required for jasmonate-regulated defense and fertility. Science **280,** 1091-1094, doi/10.1126/science.280.5366.1091.

Xu, J., Meng, J., Meng, X., Zhao, Y., Liu, J., Sun, T., Liu, Y., Wang, Q., and Zhang, S. (2016). Pathogen-Responsive MPK3 and MPK6 Reprogram the Biosynthesis of Indole Glucosinolates and Their Derivatives in Arabidopsis Immunity. Plant Cell **28,** 1144-1162, doi/10.1105/tpc.15.00871.

Xu, L., Liu, F., Lechner, E., Genschik, P., Crosby, W.L., Ma, H., Peng, W., Huang, D., and Xie, D. (2002). The SCF(COI1) ubiquitin-ligase complexes are required for jasmonate response in Arabidopsis. Plant Cell **14,** 1919-1935, doi/10.1105/tpc.003368.

Zamocky, M., Ludwig, R., Peterbauer, C., Hallberg, B.M., Divne, C., Nicholls, P., and Haltrich, D. (2006). Cellobiose dehydrogenase--a flavocytochrome from wood-degrading, phytopathogenic and saprotropic fungi. Curr. Protein Pept. Sci. **7,** 255-280, doi/10.2174/138920306777452367.

Zhang, B. and Horvath, S. (2005). A general framework for weighted gene co-expression network analysis. Stat. Appl. Genet. Mol. Biol. **4,** 6115.1128. Epub 2005 Aug 12, doi/10.2202/1544-6115.1128.

Zhang, W., Kwon, S.T., Chen, F., and Kliebenstein, D.J. (2016). Isolate Dependency of Brassica rapa Resistance QTLs to Botrytis cinerea. Front. Plant. Sci. **7,** 161, doi/10.3389/fpls.2016.00161.

Zhang, W., Corwin, J.A., Copeland, D., Feusier, J., Eshbaugh, R., Chen, F., Atwell, S., and Kliebenstein, D.J. (2017). Plastic Transcriptomes Stabilize Immunity to Pathogen Diversity: The Jasmonic Acid and Salicylic Acid Networks within the Arabidopsis/Botrytis Pathosystem. Plant Cell **29,** 2727-2752, doi/10.1105/tpc.17.00348.